

From Globular Clusters to Tidal Dwarfs: Structure Formation in the Tidal Tails of Merging Galaxies¹

Karen A. Knierman², Sarah C. Gallagher³, Jane C. Charlton, Sally D. Hunsberger

Department of Astronomy and Astrophysics

The Pennsylvania State University

University Park PA 16802

kak, gallsc, charlton, sdh@astro.psu.edu

Bradley Whitmore

Space Telescope Science Institute

3700 San Martin Drive

Baltimore, MD 21218

whitmore@stsci.edu

Arunav Kundu

Physics and Astronomy Dept

Michigan State University

East Lansing, MI 48824

akundu@pa.msu.edu

J. E. Hibbard

National Radio Astronomy Observatory

520 Edgemont Road

Charlottesville, VA 22903

jhibbard@nrao.edu

and

Dennis Zaritsky

Steward Observatory

University of Arizona

Tucson, AZ 85721

dennis@ngala.as.arizona.edu

ABSTRACT

Using V and I images obtained with the Wide Field Planetary Camera 2 (WFPC2) of the *Hubble Space Telescope*, we investigate compact stellar structures within tidal tails. Six regions of tidal debris in the four classic “Toomre Sequence” mergers: NGC 4038/39 (“Antennae”), NGC 3256, NGC 3921, and NGC 7252 (“Atoms for Peace”) have been studied in order to explore how the star formation depends upon the local and global physical conditions. These mergers sample a range of stages in the evolutionary sequence and tails with and without embedded tidal dwarf galaxies. The six tails are found to contain a variety of stellar structures, with sizes ranging from those of globular clusters up to those of dwarf galaxies. From V and I WFPC2 images, we measure the luminosities and colors of the star clusters. NGC 3256 is found to have a large population of blue clusters ($0.2 \lesssim V - I \lesssim 0.9$), particularly in its Western tail, similar to those found in the inner region of the merger. In contrast, NGC 4038/39 has no clusters in the observed region of the tail, only less luminous point sources likely to be individual stars. NGC 3921 and NGC 7252 have small populations of clusters along their tails. A significant cluster population

1. Introduction

There is growing evidence that massive young compact star clusters form in many different environments. Old globular clusters, like those seen in the Milky Way galaxy, presumably form in the early stages of galaxy formation. Recently, young compact clusters were discovered to be forming in several environments: starburst galaxies (Meurer et al. 1995), barred galaxies (Barth et al. 1995), some spiral disks (Larsen & Richtler 1999), the inner regions of mergers (Holtzman et al. 1992; Whitmore et al. 1993; Schweizer et al. 1996; Miller et al. 1997; Whitmore et al. 1999; Zepf et al. 1999) and in the space between galaxies in compact groups (Gallagher et al. 2001). Finding common characteristics between these environments may allow us to identify the mechanism that causes gas clouds to collapse and efficient star formation to begin (e.g., Jog & Solomon 1992). Also, there may be differences from environment to environment that lead to different types of “packaging” of new stars, from isolated stars, to small groups, to globular clusters, to stellar associations, to dwarf galaxies. To understand the underlying conditions responsible for the formation of these structures, it is important to identify the different environments in which they form.

Star clusters tend to form wherever vigorous star formation occurs and, especially, in starbursts triggered by galaxy interactions and mergers (Schweizer 1998). Studies with *Hubble Space Telescope* (HST) of several mergers and merger remnants show a large number of young clusters in the inner regions of the galaxies (Whitmore et al. 1993; Whitmore & Schweizer 1995; Schweizer et al. 1996; Miller et al. 1997; Whitmore et al. 1999; Zepf et al. 1999). The clusters have effective radii comparable to, but perhaps slightly larger than, the old globular clusters in the Milky Way. Their luminosity functions are best described as power laws ($\alpha \sim -2$) when expressed as the number of

clusters per luminosity bin. While this is similar to the luminosity function of globular clusters in the Milky Way for masses greater than $\sim 10^5 M_\odot$ (Harris & Pudritz 1994), merging galaxies have many more low mass clusters than found in galaxies with old globular cluster populations. This disparity could indicate a difference in the cluster formation process in primordial galaxies as compared to modern merger remnants, or it could simply indicate that evolution of the luminosity function has occurred due to fading and selective disruption (Zhang & Fall 1999).

Bridges and tails may also form during strong tidal interactions involving disk galaxies (Toomre & Toomre 1972; Barnes 1988). These tidal features have blue *UBVR* colors (e.g., $B - V = 0.53 \pm 0.13$ from Schombert, Wallin, & Struck-Marcell 1990; see also Weilbacher et al. 2000), and regions of [OII] and H α line emission have been found within the tails (Schweizer 1978; Mirabel, Dottori, & Lutz 1992; Duc & Mirabel 1998, 1999; Iglesias-Páramo & Vílchez 2001; Weilbacher, Duc, & Fritze-v.Alvensleben 2003). The inferred ages of the young stars and giant HII regions are much less than the dynamical age of the tails, indicating that star formation is occurring within the tails.

Several factors may influence star formation within tidal tails. First, the stage of the merger may be important. Secondly, 21-cm neutral hydrogen (HI) observations indicate that tails are gas rich (Yun, Ho, & Lo 1994; Hibbard et al. 2001b), and the evolution of the HI may play a role in the star formation history. Many tidal tails have associated HI which is falling back toward the center into the remnant. This infall of gas may enable star formation to continue for time scales on the order of 1 Gyr after tail formation (Hibbard & Mihos 1995). Finally, tidal dwarf galaxies are found in tidal tails in a variety of environments, particularly at the ends of the tails (Mirabel, Dottori, & Lutz 1992; Duc & Mirabel 1994; Hunsberger, Charlton, & Zaritsky 1996). These same tails that form tidal dwarfs may or may not form smaller stellar structures such as star clusters. Recent results from the early release observations of the Advanced Camera for Surveys (ACS) on HST have shown young star clusters in the tidal tails of UGC 10214 (“The Tadpole”) (Tran et al. 2003; de Grijs et al. 2003) and NGC 4676 (“The Mice”) (de Grijs et al. 2003).

¹Based in part on observations obtained with the NASA/ESA *Hubble Space Telescope*, which is operated by the STScI for the Association of Universities for Research in Astronomy, Inc., under NASA contract NAS5-26555.

²Now at Steward Obs., Univ. of Arizona, Tucson, AZ 85721; kknierman@as.arizona.edu

³Now at Center for Space Research, Massachusetts Institute of Technology, 77 Massachusetts Avenue, Cambridge, MA 02139; scg@space.mit.edu

This paper focuses on the occurrence of star clusters in the tidal tails of merging galaxies. New V and I -band observations of the tidal tails of four merging pairs obtained with HST/WFPC2 are presented. These are compared with previous observations of the inner regions of the same galaxies, and to each other, in order to consider the factors that influence the nature of the stellar systems that form in the tails. The four mergers chosen for this study span a range of dynamical states and tails with and without embedded tidal dwarf galaxies.

The four systems in this study were chosen from the “Toomre Sequence” (Toomre 1977) of ongoing mergers. This sequence is an optically selected ensemble of strongly interacting galaxies representing a suggested evolutionary sequence of disk-disk mergers, based on their stellar tidal tail lengths and the separation of the two nuclei (Toomre 1977). The four systems chosen for this study span the entire range of the sequence, from strongly disturbed, but separate, disks likely to merge (NGC 4038/39, “The Antennae”), to nearly fully merged disks (NGC 3256), to fully merged systems with single nuclei and relaxed stellar profiles (NGC 3921 and NGC 7252, “Atoms for Peace”).

In the following, Section 2 describes the HST observations, their reduction, and object selection and photometry. Section 3 presents the four mergers, with separate subsections describing the observations, the inner regions, the results, and a discussion for each. Section 4 then compares the results for the different mergers and summarizes the main conclusions.

2. Observations and Reductions

2.1. Observations

Observations of six tidal tails were obtained with HST/WFPC2 during the period Nov. 1998 to Oct. 1999, as listed in the journal of observations in Table 1. Total integration times ranged from 1000–2000 s in V (F555W filter) and in I (F814W filter). The integrations were chosen to obtain images to a depth similar to the observations of the inner regions. A gain of $7e^-/\text{DN}$ was used in all cases. At least two separate exposures in each filter were obtained to facilitate removal of cosmic rays. The positions of the WFPC2 field of

view is superimposed on optical images of the four mergers in Figure 1. The six V -band images are presented in Figures 2 – 7.

Pairs of exposure were taken of all systems except NGC 3256. The exposures were offset by $0.25''$ (i.e. 2.5 pixels on the Wide Field Camera [hereafter WF] and 5.5 pixels on the Planetary Camera [hereafter PC]). Pipeline-reduced images for each filter were averaged and cleaned using the IRAF⁴ tasks GCOMBINE. The tasks COSMICRAYS was used to remove hot pixels.

2.2. Object Detection

Objects in the images were detected using the DAOFIND task in the DAOPHOT package using a threshold of 2.0 counts per object, finding objects greater than 2σ above the local sky background. The noise was determined from the sky annulus of 5 to 8 pixels around each object identified by DAOFIND and only objects with a signal-to-noise per object greater than 3 were retained. For images with multiple exposures, the objects were detected separately in each pointing. Then the two source lists were matched using the offsets calculated from bright stars. Only those sources with detections in both the V and I filters were retained.

Only point-like sources are of interest in this paper, as extended objects will be addressed in a future study. In addition to possible star clusters, this method detects foreground stars and compact background galaxies. We use a classification based upon the $V - I$ color and a structural parameter. To obtain a sample of possible star clusters, we keep only those sources with $V - I < 2.0$. Old, metal-poor globular clusters in the Milky Way have $V - I \sim 1$ (Reed, Hesser, & Shawl 1988), so this cut would not exclude old clusters. The most metal-rich clusters, from observations of the Milky Way and nearby elliptical galaxies, have $V - I < 1.5$ (Peterson 1993; Ajhar, Blakeslee, & Tonry 1994; Whitmore et al. 1995; Kundu & Whitmore 2001a,b). Stellar population models by Lee, Lee, & Gibson (2002) which take into account the effect of the horizontal branch on colors show that even solar metallicity globular

⁴IRAF is distributed by the National Optical Astronomy Observatories, which are operated by AURA, Inc., under contract to the NSF.

clusters only have $V - I \sim 1.2 - 1.3$. Also, only those sources with $V_{err} < 0.25$ were retained.

As in Whitmore et al. (1993) and Miller et al. (1997), we calculated the concentration index, the difference in V magnitude between an aperture of 0.5 pixel radius and an aperture of 3.0 pixel radius, denoted by $\Delta_V(0.5 - 3)$. A sky annulus of 6 to 9 pixels was used to subtract the background. For each system, we used a different concentration index. In the NGC 3256 images, we classified objects with $\Delta_V(0.5 - 3) > 2.4$ as diffuse and removed them from the sample. The cutoff for the concentration index was raised to 3.0 for NGC 4038/39, the closest system, to avoid eliminating any possible clusters.

For NGC 3921 and NGC 7252, we modified the above photometry method to probe deeper apparent magnitudes for comparison with the central regions and larger sized objects, such as the stellar associations found close to the central regions of NGC 3921 (Schweizer et al. 1996). For these images we used DAOFIND with the threshold set at 1.5 rather than 2.0 as above. The signal-to-noise was calculated again, this time using a cutoff of 1.5 per object. As above, we retained sources with $V - I < 2.0$ and $V_{err} < 0.25$. There was no cutoff for concentration index. By removing the size criteria for objects in these mergers, we retained more diffuse sources which we could compare with the stellar associations from Schweizer et al. (1996).

For each tail, a region in the V -band image was manually identified as "in-tail", corresponding to contiguous regions with ~ 1 count (DN) above the background (corresponding to a V magnitude surface brightness of $24.3 - 25.7$ mag arcsec $^{-2}$ according to the specific tail). All other regions were designated as "out-of-tail". In Figures 2-7, "in-tail" point sources are indicated by open circles, while "out-of-tail" point sources are indicated by open squares.

2.3. Completeness

Figure 8 shows the completeness fraction on the wide-field chips for the observations of NGC 3256W. The completeness was determined by adding 10,000 stars (100 at a time to avoid crowding) using the ADDSTAR program within the DAOPHOT package. The surface brightness of

the tail is so low (~ 1 DN above the background) that a single background level is sufficient for characterizing the completeness fractions, rather than the multiple curves used in other studies with a wide variety of backgrounds (Whitmore et al. 1999, e.g.). We find that the completeness fraction reaches $\sim 50\%$ at $V = 25.8$, or 25.4 corrected for foreground extinction, consistent with our visual estimate of the completeness correction from the color magnitude diagram for NGC 3256W (see Figure 11). Comparison of the color magnitude diagrams indicates that the completeness limits for NGC 3921 and NGC 4038/39 are similar to that for NGC 3256. For NGC 7252, our slightly relaxed detection criterion (see § 2.2) yields a slightly deeper completeness limit, by ~ 0.2 magnitudes.

For several reasons, few sources were detected on the PC chip in any of the fields (8 in the NGC 3256W PC, 2 in the NGC 3256E PC, and none in any others). First, the fields were positioned for maximal total coverage of the tail regions, from which it follows that the tails do not pass through the PC chip. Second, the area covered by the PC chip is smaller than a single WF chip. Finally, in the PC chip the light is spread over a larger number of pixels, but the read noise is the same per pixel. We are working in a regime where read noise is important, thus the detection limit is not as faint for the PC as for the WF (see Whitmore et al. (1999) for a similar comparison). Therefore, only WF observations will be discussed in this study. PC sources have not been plotted in Figures 2-7.

2.4. Photometry

Photometric zeropoints were adopted from Table 28.1 of Version 3 of the *HST Data Handbook* (Voit 1997). The Holtzman et al. (1995) photometric transformation corrections were applied (to convert from the HST filter system to Johnson-Cousins).

Aperture photometry was performed on all pointlike objects in the cleaned images using the PHOT task in the APPHOT package. The radii of the object aperture, the inner boundary of the background annulus, and the outer boundary were 2/5/8 pixels for the WF. For all fields, the aperture corrections $V = 0.28$ and $I = 0.31$ were adopted. These were an average of those derived for stars in the three WF chips for NGC 1700 and NGC 3610

(Whitmore et al. 1997), which were calibrated using point sources in the NGC 5139 (ωCen) and NGC 6752 fields. Ideally, we would have used cluster candidates in our own fields to determine aperture corrections, however this procedure was subject to large uncertainties due to a lack of sufficiently bright sources. For the best case, WF2 in the NGC 3256W image, nine bright stars were used to determine corrections of 0.276 ± 0.014 in V and 0.293 ± 0.006 in I . These are consistent with our adopted values. For the nearest pair, using stellar aperture corrections (instead of clusters) introduce a systematic error of only a couple hundredths of a magnitude, insignificant for the purpose of this study.

The foreground extinction due to the Galaxy was corrected for each pair using the A_B values from Schlegel, Finkbeiner, & Davis (1998) and the reddening curve from Mathis (1990). The A_B values for each merger are listed in Table 2. We corrected for non-optimal charge-transfer efficiency (CTE) using the formulae of Whitmore, Heyer, & Casertano (1999).

3. The Four Merging Pairs

For each of the mergers we will summarize past observations of the inner regions, present new HST observations, and discuss our results. Figure 1 shows optical images of the four mergers, with HI contours, and with the locations of the six observed WFPC2 fields superimposed. Table 2 presents a comparison of tail properties including velocity of merger, distance modulus, extinction in B magnitudes (A_B), length from the central region along the tail to the position where the image begins (l), physical scale of tail region encompassed in the image (Δl), absolute magnitude for 50% completeness limit ($M_{V,50\%}$), HI mass of tail ($M_{HI,tail}$), and the approximate age of tail (the projected length of the tail divided by the rotational or escape velocity). The mergers are discussed in increasing order of their place in the Toomre Sequence.

3.1. NGC 4038/39 (“The Antennae”)

The Antennae is one of the best known and earliest modeled merger systems (Toomre & Toomre 1972; van der Hulst 1979). It is the nearest of the four mergers in this study (see Table 2).

Its long, nearly symmetric crossed tidal tails and still-separate nuclei indicate a relatively young, strongly interacting merger; see Figure 1 for an optical image. The southern tail is longer than the northern one and features a putative dwarf galaxy at the tip (Schweizer 1978; Mirabel, Dottori, & Lutz 1992). Images in $H\alpha$ of NGC 4038/39 show vigorous star formation within the main disks (Whitmore & Schweizer 1995). The optical spectrum, with a blue continuum and strong emission lines, is indicative of an active star-forming galaxy. The equivalent width of the $H\alpha$ line is 2–3 times higher than the normal average of $\sim 25 \text{ \AA}$ in an average Sb or Sc galaxy, categorizing NGC 4038/39 as a starburst galaxy (Kennicutt 1992).

The southern tail is rich in HI, while the northern is HI-poor. HI contours overlay the optical image in Figure 1 (from Hibbard et al. 2001a). At the end of the southern tail lie at least three HII regions. A spectrum from Mirabel, Dottori, & Lutz (1992) shows that this region has a low O/H abundance, which is typical for dwarf galaxies. The region at the tip of the tail also shows a high concentration of HI (van der Hulst 1979; Hibbard et al. 2001a).

We use the maximum projected tail length of 65 kpc (Schweizer 1978, corrected for our adopted distance) and the disk rotation speed of 150 km s^{-1} inferred from the Fabry-Perot observations of Amram et al. (1992, corrected for disk inclination), to infer an interaction age of $65 \text{ kpc} / 150 \text{ km s}^{-1} = 420 \text{ Myrs}$. This age, measured from orbital periaapse when the tails were launched, is in excellent agreement with the best match time of 450 Myrs from the numerical model of NGC 4038/39 run by Barnes (1988). It is also remarkably close to the age of the population of 500 Myr old globular clusters found by Whitmore et al. (1999) (see also Fritze-v. Alvensleben 1998), supporting the hypothesis that this globular cluster population formed around the time when the tails were first ejected (Whitmore et al. 1999).

3.1.1. Inner Region

Whitmore et al. (1999) found young globular clusters in the inner regions of the Antennae. More than 14,000 point-like objects were identified in the field, of which most were probably young stars formed in the merger. Depending on selection cri-

teria, the number of young compact star clusters is between 800 and 8000. Remaining sources are individual supergiant stars, also in the Antennae. The luminosity function is composed of two power law segments with a bend at $M_V \sim -10.4$. The median effective radius of the young clusters is 4 ± 1 pc, just slightly larger than the 3 pc radius for Milky Way globular clusters (van den Bergh 1996). The ages of the young clusters range from less than 5 Myr up to 100 Myr. There are also populations of intermediate age (500 Myr) and of old globular clusters (Whitmore et al. 1999).

3.1.2. Observations of the Southern Tail

Three observations were planned for this merger, but only one has been included in this study. In Figure 1, the WFPC2 field of view is overlaid on an optical image of NGC 4038/39. The WFPC2 image was obtained on 1999 Feb 22 (see the V -band image in Figure 2). Two later observations, not analyzed here, are indicated by the lighter boxes in the image. At the distance modulus of 31.4 (for $H_0 = 75$ km/s/Mpc; as in Whitmore et al. 1999), the limiting magnitude (50% completeness) of $m_V \sim 25.8$, consistent with our visual estimate of the completeness correction from the color magnitude diagram (CMD), corresponds to an absolute magnitude limit of $M_V \sim -5.8$. Despite the closeness of this merger, a long exposure was obtained (see Table 1) to match the depth of existing images of the inner regions. Therefore, these NGC 4038 images are far deeper in absolute magnitude than those of the other mergers presented in this paper. In addition to our image along the middle of the Southern tail, HST/WFPC2 observations of the candidate tidal dwarf galaxy at the tip of the Southern tail were obtained by Saviane, Hibbard & Rich (2003). Their image is 2 magnitudes deeper than our limiting magnitude.

3.1.3. Results

A $V - I$, V color magnitude diagram (CMD) is presented in Figure 9. The plot only includes the range $-0.75 < V - I < 2.0$ since we do not expect to see clusters with $V - I > 2.0$. In the inner region of NGC 4038/39, clusters identified by Whitmore et al. (1999) have an $M_V < -9$ (indicated by the dotted line in Figure 9) and colors $0.0 < V - I < 0.6$, with a particular concentration at $-12 < M_V < -10$ and $0.3 < V - I < 0.4$

(Whitmore et al. 1999). Of the sources in the tail, none lie in the same region of the CMD where Whitmore et al. (1999) discover clusters, as shown in Figure 9. The tail sources are fainter and/or redder. The grouping of ~ 30 sources in the tail CMD falls in the same area as individual stars in the inner region of the Antennae ($M_V > -9$ and $-1.0 < V - I < 1.0$; Whitmore et al. 1999). Many of these are probably isolated red or blue supergiants. Whitmore et al. (1999) use U and B images to help separate stars from the cluster population, however we have only V and I images.

Since the “in-tail” and “out-of-tail” regions in this field are equal in area, it is noteworthy that there are a larger number of faint sources in the tail regions (42 vs. 24 in the “out-of-tail” regions). However, there is no significant difference between the distribution of sources in the CMD for sources in and out of the tail (Figure 9). The probabilities of the magnitudes and colors being drawn from the same distributions are 0.27 and 0.89, respectively, by the Kolmogorov–Smirnov test (Press et al. 1986). In Figure 10, the $V - I$ color is plotted versus the concentration index, but again there is no difference in the distributions for sources in and out of the tail ($P(KS) = 0.89$ for the color and 0.71 for the concentration index distribution).

3.1.4. Discussion

As seen in Figure 2, some of the fainter point sources lie along the optical tail. However, there is an absence of bright ($M_V < -9$), young clusters compared to the inner region. If clusters formed only concurrent with the tail, ~ 450 Myrs ago, they should still be detected in the CMD (see Figure 9). This is evident since 21 $M_V < -9$ sources of intermediate ages were found by Whitmore et al. (1999) in their comparable exposure of the body of the NGC 4038/39 merger and its inner tail regions. In fact, many of the fainter sources that we find within the tail may be individual red and blue supergiants, perhaps forming in the tail.

This image was taken ~ 30 kpc from the inner region and contains ~ 20 kpc of the Southern tail. It is possible that other regions of the tails do have cluster populations. Whitmore et al. (1999) identified about a dozen objects in the inner part of the Southeastern tail, but only one of them was bright enough ($M_V = -9.48$) to be

definitively identified as a cluster. Our additional observations include the Northern tail, which has less H I by a factor of five (van der Hulst 1979; Hibbard et al. 2001a), and another region in the Southern tail which is closer to the inner region. These images provide the opportunity to study the distribution of clusters in the tail and the relationship of the H I content to the characteristics of the cluster population. The candidate tidal dwarf galaxy at the tip of the Southern tail has 8 extended young star clusters, 5 of which are brighter than $M_V = -8.5$ and many young blue stars fainter than $M_V = -8.5$ (Saviane, Hibbard & Rich 2003). At least the tip of the Southern tail of NGC 4038/39 contains star clusters.

3.2. NGC 3256

NGC 3256 is intermediate in the “Toomre Sequence,” and it is the second nearest merger in this study. The inner region has structures such as loops, knots, and dust lanes usually seen in mergers, as well as sweeping, symmetric tidal tails (see the optical image in Figure 1). In radio continuum observations, two nuclei can be seen, separated by ~ 1 kpc (Norris & Forbes 1995). Of the “Toomre Sequence” mergers, NGC 3256 has the most molecular gas, $1.5 \times 10^{10} M_\odot$ (Casoli et al. 1991; Aalto et al. 1991; Mirabel et al. 1990), and is the brightest in the far-infrared, with $L_{FIR} = 3 \times 10^{11} L_\odot$ (Sargent, Sanders, & Phillips 1989). In addition, NGC 3256 is the most X-ray luminous starburst known, with $L_{0.5-10\text{keV}} = 1.6 \times 10^{42} \text{ ergs s}^{-1}$ (Moran, Lehnert, & Helfand 1999). The tails have rich H I content but no tidal dwarf candidates have been discovered within them (English et al. 2003, see the H I contours in Figure 1).

The approximate dynamical age of NGC 3256 is calculated in a similar manner as for NGC 4038/39 (presented in §3.1). However, for a face-on orientation the maximum velocity is best represented by the escape velocity, 150 km s^{-1} (English & Freeman 2003), and the tail age is estimated to be $61 \text{ kpc}/150 \text{ km s}^{-1} = 400 \text{ Myr}$.

3.2.1. Inner Region

In WFPC2 images, Zepf et al. (1999) find more than 1000 compact, bright blue objects in the inner regions of NGC 3256. This population has

colors, luminosities, and sizes similar to those of young globular clusters, with ages from a few to several hundred Myr. The luminosity function can be fit with a power law. The young cluster population is quite extreme in that it comprises $\sim 20\%$ of the total blue luminosity of the galaxy. This could indicate a high global efficiency of cluster formation.

3.2.2. Observations of the Western and Eastern Tails

In Figure 1, the WFPC2 field of view is overlaid on an optical image of NGC 3256. The V and I -band images of the Western tail were obtained on 1999 Mar 24, and we present the V -band image in Figure 3. The images of the Eastern tail, obtained on 1999 Oct 11, are represented by the V -band image in Figure 4. The 50% and 90% completeness limits correspond to $M_V = -7.5$ and $M_V = -8.7$.

3.2.3. Results

The observations of the inner region from Zepf et al. (1999) were obtained in the B and I bands, which precludes a direct comparison with our observations in V and I . From the V -band WFPC2 images of the Western and Eastern tails in Figures 3 and 4, it can clearly be seen that the density of objects is higher within the tail regions. In addition, both the Western and Eastern tails show a grouping of sources in the CMD at $-10 < M_V < -7$ and $0 < V - I < 1$, which is more prominent in the “in-tail” than in the “out-of-tail” regions (see Figure 11). For the Western tail, the Kolmogorov-Smirnov (K-S) statistic indicated that the probabilities that the magnitude and colors of “in-tail” and “out-of-tail” sources are drawn from the same population are, 0.03 and 2.2×10^{-6} , respectively. For the Eastern tail, the statistical significance of the difference is not as large. The magnitudes have a K-S probability of 0.20 of being drawn from the same distribution, but the color distributions are different at $> 2\sigma$ significance. Some of the fainter sources could be individual stars, but the majority are likely to be clusters (Whitmore et al. 1999). In the Western tail, there are 71 sources falling in the region of the CMD defined by $-10 < M_V < -7$ and $0 < V - I < 1$. The Eastern tail has 25 sources in this region. Outside the tail, there are only 29

sources in the Western image and 8 in the Eastern image that fall within this same region of the CMD.

The cluster candidate sample is contaminated by foreground stars since NGC 3256 is at a low galactic latitude ($b = +11.7$). Examination of the concentration index can aid in separating the clusters from the stars. The concentration index for blue sources ($V - I < 1.1$) within the Western tail (Figure 10) is peaked at ~ 1.8 , while for red sources ($V - I > 1.1$) out of the tail, the peak is ~ 1.5 . Hence the clusters (blue objects) appear to be resolved compared to the stars (red objects). By the K-S test, these distributions have a probability of 0.06 of being drawn from the same distribution of concentration index, but the distributions of colors differ at $> 5\sigma$. There is a grouping of sources in the concentration index plot at a large concentration index which is composed of the same sources as the grouping at $0 < V - I < 1$ in the CMD.

Candidate cluster sources in the Eastern tail are less numerous than those in the Western tail, but many of them are in the same region of the CMD and the concentration index plot as those Western sources that have been identified as clusters. In the Western tail, there is a clear separation in concentration index between “in-tail” and “out-of-tail” sources. The sources in the Eastern tail have less separation, no significant difference in the distribution of concentration index by the K-S statistic ($P(KS) = 0.84$), and a 2σ difference in the distributions of color.

The majority of clusters in the Eastern tail, 18 out of 25, appear in WF2, which includes the part of the tail closest to the center. In the Western tail, the majority of clusters, 43 out of 71, appear in WF4, compared to 25 in WF2, the other significant contributor. In this case, WF4 contains the part of the tail farthest from the center.

3.2.4. Discussion

From the CMD (Figure 11) and the concentration index diagram (Figure 10) for the Western tail, we infer that most of the sources with $-10 < M_V < -7$ and $0 < V - I < 1$ are star clusters. The peak of the color distribution is $V - I \sim 0.5$. The majority of clusters in the Western tail are in the outer higher surface brightness

regions of the tail.

There are fewer clusters in the Eastern tail and the majority of them are closer to the inner regions. The Eastern tail appears to be of higher surface brightness toward the center, following the distribution of clusters. In addition to more star clusters, the Western tail has a higher H I mass than the Eastern tail ($2.2 \times 10^9 M_\odot$ vs. $1.4 \times 10^9 M_\odot$; English et al. 2003).

Ages of clusters can be estimated using the evolutionary tracks for a $10^5 M_\odot$ instantaneous burst (Bruzual & Charlot 1993; Charlot, Worthey, & Bressan 1996)⁵ with solar metallicity and a Salpeter IMF, superimposed on the CMDs in Figure 11. A range of cluster masses, $\sim 10^4 - 10^5 M_\odot$, would allow for a population with the range of ages, 30–300 million years, to explain most of the observed M_V and $V - I$. However, the bluer clusters (those with $V - I < 0.3$) require either a lower metallicity (see Schweizer et al. 1996) or considerably younger populations (several million years old). Regardless, it would appear that the clusters are younger than the tail in which they formed. Therefore, they were not pulled out into the tail from inner regions, but rather they formed “in situ” in dense H I regions within the tail.

3.3. NGC 3921

NGC 3921, the second to last of the “Toomre Sequence”, features a single nucleus, a main body with ripples and loops, and a pair of crossed tidal tails. The two galaxies have essentially merged (Figure 1; see also Schweizer 1996). The southern tail extends below the main body, ending in large concentration of H I, possibly a tidal dwarf galaxy (Hibbard & van Gorkom 1996). NGC 3921 is the most distant merger in our sample of four.

Consistent with an evolved merger, the optical spectrum is dominated by Balmer absorption lines, a classic post-starburst signature (Kennicutt 1992). NGC 3921 shows no H I in the northern tail while the southern tail is gas-rich (see the H I contours in Figure 1). This difference in H I between the tails may indicate the merger of two different types of galaxies, a gas-rich, late-spiral type and a gas-poor, early-type disk galaxy. The approximate tail age of NGC 3921, calculated as

⁵Taken from http://www.stsci.edu/instruments/observatory/cdbs/cdbs_bc95.html

in §3.1, is $64 \text{ kpc}/140 \text{ km s}^{-1} = 460 \text{ Myr}$ (Hibbard & van Gorkom 1996).

3.3.1. Inner Region

In WFPC2 images obtained by Schweizer et al. (1996, hereafter S96), there are two chains of point-like candidate globular clusters and more extended stellar associations along the inner part of the southern tail, as well as several slender, narrow arcs of these sources. Their HST image reveals ~ 100 candidate globular clusters and ~ 50 stellar associations. The globular clusters tend to be more centrally located while the associations trace the southern loop and two tidal tails.

The majority of the inner region’s clusters and associations are blue and have rather uniform colors with a median $V - I = 0.65$ for globular clusters and 0.56 for associations. Depending on the metallicity, the ages of the globular clusters range from $250\text{--}750 \text{ Myr}$ with an upper limit on their radii of 5 pc . The luminosity function of the globular clusters and that of the associations are represented by power laws. S96 estimate that the number of globular clusters increased by greater than 40% during the merger.

3.3.2. Observations of Southern Tail

In Figure 1, the WFPC2 field of view is overlaid on an optical image of NGC 3921 (see Table 1 for exposure information). The images of the Southern tail, obtained on 1999 Apr 30, are represented by the V -band image in Figure 5. With a distance modulus of 34.5 (for $H_0 = 75 \text{ km/s/Mpc}$; S96), our source catalog for NGC 3921 is 50% complete to $m_V \sim 25.8$, consistent with our visual estimate of the completeness correction from the CMD, which at this large distance corresponds only to $M_V = -8.7$.

3.3.3. Results

Because our image partially overlaps with the observation by S96, we compare three globular cluster and five stellar association candidates found in that paper which correspond to our sources. These eight sources have a range in brightness of $23.5 < V < 25.4$ and a range in color of $-0.2 < V - I < 1.1$. The mean difference between the S96 data and our data is 0.12 magnitudes for $V - I$ and 0.43 magnitudes for V . The

S96 values are consistently fainter than our values and slightly redder on average. The differences between the data appear to be due to the differences in the corrections for finite aperture size, charge-transfer efficiency (CTE), and reddening. For sources on the WF chips, S96 used a 1 pixel aperture for aperture photometry, while our procedure used a 2 pixel aperture. This would cause more extended sources, or stellar associations, to have a larger difference between the two data sets than the less extended sources since a single aperture correction has been made for all sources. In our comparison, the five associations have a mean difference of 0.55 mag in V and 0.12 mag in $V - I$ while the cluster candidates have a mean difference of 0.23 mag in V and 0.09 mag in $V - I$. Corrections for CTE problems were not made by S96 due to the varied background in their images. Our calculations include corrections for CTE, at times as large as -0.2 magnitudes for faint sources near the top of the chip. S96 used $A_V = 0.00$ to correct for foreground Milky Way extinction, whereas we used $A_V = 0.046$. As an independent check on their photometry, S96 compared their photometry performed with VISTA software with photometry using IRAF software. The objects measured in IRAF were found to have a mean difference in $V - I$ of 0.08 mag bluer than the objects measured in VISTA, possibly due to different centering algorithms or different aperture corrections. Regarding V magnitudes, S96 estimate that larger associations may have V magnitudes up to several tenths of a magnitude brighter, due to their more extended profile. Hence, taking into account differences in corrections for aperture size, CTE, and reddening, we find our values for photometry to be consistent with the S96 photometry.

As shown in Figure 12, there are few sources seen in the tail of this system. S96 find a population of bright clusters in the inner region with a narrow color range at $V - I = 0.65$, indicated by the horizontal dotted line in Figure 12. Sources in the tail do not appear to be clustered around this line, indicating that there is not a large population of clusters of the same age in the tail. The K-S test shows no significant difference between the distributions of color and magnitude ($P(KS) = 0.98$ and 0.05) for sources in the tail compared to those out of the tail.

The associations that overlap with S96 fall in

the same region of the CMD, $-11 < M_V < -9$ and $-0.1 < V - I < 0.9$. There are a few additional sources in the tail that also fall in this region of the CMD, and most of these lie closer to the inner region of the merger.

In a first pass through the photometry, only point sources were kept, using the method outlined in §2.4. This method yielded very few sources and missed several of the associations identified in S96. When the criteria were relaxed, as outlined in §2.2, many more extended objects were found. Most of those found off the tail may be background galaxies, but those within the tail have properties consistent with the stellar associations found in S96. At this distance one WF pixel corresponds to 39 pc, so it is difficult to distinguish clusters from stars using the concentration index.

The putative tidal dwarf galaxy was imaged in the PC. It appears to be a low surface brightness dwarf and no point sources were found within it. However, there are four knots within the more diffuse emission which extends over about 7 kpc. This tidal dwarf galaxy candidate will be addressed in a future study of the extended sources within these tails.

3.3.4. Discussion

Most of our sources that are in the same region of the CMD as those from S96 are located in the region closer to the main body of the merger and are bluer than sources elsewhere in the field. Most of the bluer sources in the tail have a large concentration index, indicating the possible presence of larger, stellar associations. In addition to these large associations, there is a putative dwarf galaxy centered in the PC. There is an absence of point sources in the optical tail at larger distances from the main body of the merger.

3.4. NGC 7252 (“Atoms for Peace”)

As the system located at the end of the Toomre Sequence, NGC 7252 exemplifies the prototypical merger remnant (see the optical image in Figure 1). It is the second most distant of the four mergers in our sample. Schweizer (1978, 1998) defines some characteristics of a recent merger remnant: a pair of long tidal tails, isolated from neighbors, a single nucleus, tails moving in opposite directions relative to nucleus, and chaotic motions

in the main body of the merger, all of which NGC 7252 possesses (Schweizer 1982). The central region of this remnant has a single nucleus with several loops. Observations with HST have revealed a mini-spiral structure in the inner region which coincides with the disk of molecular and ionized gas (Wang, Schweizer, & Scoville 1992; Whitmore et al. 1993; Miller et al. 1997). The long, straight tails extend from the body of the remnant to the east and northwest, each ending in a concentration of H I associated with a candidate tidal dwarf galaxy. The outer parts of both tails have blue $B - R$ colors, with the bluest parts coincident with the highest gas density (Hibbard et al. 1994).

The tails of NGC 7252 and the western loop region are both rich in H I (see the H I contours in Figure 1). The kinematics of the northwestern tail suggest that the material at the base of the tail is falling into the main remnant (Hibbard & Mihos 1995). This infall could explain some of the peculiar ripples and shells associated with the center. The presence of a young, metal poor emission line cluster in the western loop (15 kpc from the center), is consistent with recent star formation that is perhaps triggered by infalling metal poor gas from the tail (Schweizer & Seitzer 1998). The approximate tail age of NGC 7252, calculated as in §3.1, is $160 \text{ kpc}/220 \text{ km s}^{-1} = 730 \text{ Myr}$ (Hibbard et al. 1994) which is in good agreement with the age of 770 Myrs as determined through numerical modeling (Hibbard & Mihos 1995, correcting to $H_0 = 75 \text{ km/s/Mpc}$).

3.4.1. Inner Region

WFPC2 observations of the inner regions of NGC 7252 detected ~ 500 cluster candidates which separate into three populations. Luminous, blue clusters with a narrow color range $V - I \sim 0.65$, have ages around 650–750 Myr. They were likely to have formed around the time that the tails were launched. These clusters have an upper size limit of $4.8 \pm 0.4 \text{ pc}$. The inner disk is home to a population of very young ($\sim 10 \text{ Myr}$) clusters with $U - B$ colors indicating that O stars dominate and with radii of $8.3 \pm 0.6 \text{ pc}$. The third population consists of the older, metal-poor globular clusters from the original galaxies. The combined luminosity function of these populations of clusters is a power law with $\alpha \sim -1.8$ (Miller et al. 1997).

3.4.2. Observations of Western and Eastern Tails

In Figure 1, the WFPC2 fields of view are overlaid on an optical image of NGC 7252 (see Table 1 for exposure information). The images of the Western tail, obtained on 1998 Nov 18, are represented by the V -band image in Figure 6. The Eastern tail observations, obtained on 1999 Aug 29, are represented by the V -band image in Figure 7. With a distance modulus of 34.0 (for $H_0 = 75$ km/s/Mpc; Schweizer 1982), the detection limit of $m_V \sim 26.0$ (50% completeness), consistent with our visual estimate of the completeness correction from the CMDs, corresponds to $M_V = -8.1$.

3.4.3. Results

The clusters in the inner region identified by Miller et al. (1997) include populations of intermediate and old clusters at $V - I = 0.65$ and 1.0, as indicated by the horizontal dotted lines on the CMD in Figure 13. The blue clusters have $19 < V < 25$. There are also some bright, blue clusters with $V - I < 0.6$ (Miller et al. 1997), found mostly within the inner $6''$ of the galaxy.

The Western tail CMD shows a possible enhancement of bluer, faint sources at $-12 < M_V < -8.5$ and $0.2 < V - I < 1.0$ (Figure 13), which are located in the tail region. The K-S test yields a difference at a 2σ level between the colors for “in-tail” and “out-of-tail” sources, but no significant difference in their magnitude distributions. Seven members of the group at $0.2 < V - I < 0.65$, noted as star symbols on the CMD, are located in the putative tidal dwarf galaxy. A close up of the V -band image of this region with the seven star clusters indicated is shown in Figure 14. The several sources with $0.65 < V - I < 1.0$ are spread through the optical tail.

For the Eastern tail, Figure 13 shows a small group of sources in the tail at $M_V \sim -9$ and $0.2 < V - I < 1.2$. However, this concentration is not different from the grouping in the CMD of sources not in the tail. There is only one bright candidate ($M_V < -9$) in the tail region, while the region outside the tail hosts several such bright sources at $V - I \sim 0.5$. The nature of these sources is ambiguous. The K-S statistic shows no significant difference in either the magnitude or the

color distributions for “in-tail” and “out-of-tail” sources. The concentration index is less useful for this merger because it is so far away (1 WF pixel is 31 pc). There are two sources in the Eastern tail dwarf which are quite blue ($V - I < 0.3$), noted as three-pointed star symbols on Figure 13; see Figure 14 for a V -band image of the dwarf.

3.4.4. Discussion

Although there are several blue sources with $V - I < 1.0$ in the Eastern and Western tail regions, there is no convincing evidence for an excess over the “out-of-tail” regions, with the important exception of clusters within the prominent tidal dwarf candidates in each tail.

The tidal dwarf candidate in the Western tail is clumpy, consisting of several knots spread over ~ 1 kpc and embedded in extended high surface brightness material. There are seven clusters found within it and they are relatively blue. Their concentration indices are somewhat larger (2.2–3.0) than the mean of 1.8 for the tidal cluster sources, but they are still consistent with being clusters at this distance. However, the measurement of the concentration parameters for clusters in this tidal dwarf candidate is uncertain since it is a crowded environment. These clusters in the Western tidal dwarf candidate are grouped together in the CMD (star symbols in Figure 13) and their average $V - I$ color is 0.4, bluer than the major population of clusters in the inner regions of NGC 7252. The CMD suggests an age of less than 100 Myrs, which is less than the formation age of the tail, and as such the clusters formed within the tidal debris.

Hibbard et al. (1994) found strong kinematic evidence for a mass concentration at the location of the putative tidal dwarf in the western tail of NGC 7252. This evidence consisted of an increase in the H I linewidth centered on and symmetric with the concentration of gas, light, and star forming regions associated with the tidal dwarf galaxy. The appearance of star clusters at this location, especially since there is no statistically significant excess of star clusters elsewhere in the tail, is further evidence in support of this region being dynamically distinct.

The tidal dwarf in the Eastern tail is almost featureless and of only slightly higher surface bright-

ness than the tail. The several clusters within the dwarf are among the bluest in the sample. They are consistent with the very blue colors of those clusters within the inner 6'' of NGC 7252. These inner region clusters have an age of ~ 10 Myr. Though the clusters could have formed recently, the dwarf itself may have formed earlier.

The contrast in the distribution of young stars in the two candidate dwarf galaxies is striking. The Western tail dwarf is of higher surface brightness and contains several blue clusters in close proximity, and the Eastern tail dwarf is almost featureless, with only two clusters spaced farther apart. In the Eastern tail dwarf, the extreme blue colors indicate that the clusters are considerably younger than the age of the interaction. A similar situation is found in the Northern Starburst region of Stephan's Quintet, one of Hickson's compact galaxy groups. That region is separated from the nearest giant galaxy by more than 25 kpc, yet it hosts a very young stellar population (less than 5 Myr; Gallagher et al. 2001). It will be interesting to compare the range of properties of these and other tidally formed dwarfs to the varied population of compact and diffuse dwarf galaxies in the Local Group.

4. Summary and Discussion

In our study of six HST WFPC2 images of six tidal tails in four merging pairs, we found evidence for extreme differences in cluster formation among the tidal tails. To compare the debris in the different mergers on equal footing, we must consider contamination by foreground and background objects and the relative areas of "in-tail" and "out-of-tail" regions (fractions f_{in} and f_{out}). We must also consider selection effects due to the different distances of the pairs. Table 3 gives the "in-tail" and "out-of-tail" source densities in each tidal tail, for sources with $V - I < 0.7$ and with $M_V < -8.5$. The latter criterion was chosen because sources this bright are likely to be clusters rather than individual stars. Table 3 also lists the specific frequencies of young clusters, S_{young} , for each tail region, defined as the number of young clusters per $M_V = -15$ luminosity (in a similar way to how Harris (1991) defined the specific frequency for old globular clusters).

Figure 15 gives, for the six regions, the differ-

ences in the source densities in and out of the tails. This is a way of subtracting the background, but it neglects the fact that some "out-of-tail" sources might be real clusters. Errorbars are simply from Poisson statistics; if some of the objects outside of the tails are clusters then the background subtraction is systematically too large and the surplus found would represent a lower limit.

The Western tail region of NGC 3256 shows a significant excess of sources likely to be star clusters. The five other regions show a much smaller number, consistent with 0 for NGC 4038 and NGC 7252E, but statistically significant for the other three tail regions, NGC 3256E, NGC 3921, and NGC 7252W. In the case of NGC 3921, many of the sources in the Southern tail are stellar associations also reported by S96. By having different detection criteria for NGC 3921 and NGC 7252, we attempted to find any faint clusters that might add to the numbers such that these regions might compete with the number of clusters found in NGC 3256W. Since we did not find a population of faint sources in the tails of NGC 3921 and NGC 7252, the excess of sources in NGC 3256W is even more significant. If we just look at the brightest sources in all the tails which have $M_V < -9.0$ and $M_V < -9.5$ (with $V - I < 0.7$, as above), NGC 3256W still has a much larger excess of clusters within the tail.

While the the tails of NGC 7252 generally lack clusters, it is remarkable that there is a population of clusters associated with both tidal dwarf candidates (seven in the western dwarf, two in the eastern one). The two tidal dwarf candidates show different populations of clusters, however, with the Eastern dwarf bluer than the Western dwarf. For the Western tidal dwarf, the clusters may have formed either before or concurrent with the dwarf. The Eastern dwarf probably formed prior to its recent burst of star formation. Though differential reddening could induce the observed color differences between the two dwarfs, we have no evidence which suggests this might be the case.

The NGC 4038 tidal debris shows no large young cluster population like that observed in its inner regions. There are fainter objects, which could be individual young stars within the tail, but there are only 3 objects brighter than $M_V = -9$, the cutoff for clusters used by Whitmore et al. (1999), and all of these have $V - I > 1$. At least

this section of the tail, if not the entire tail, has few, if any, clusters. Interestingly, HST/WFPC2 images of the region of the tail coincident with the tidal dwarf candidate (Saviane, Hibbard & Rich 2003) show 8 young stellar associations in the vicinity of the tidal dwarf. The high concentration of blue star clusters in the vicinity of a tidal dwarf candidate, but general lack of such clusters elsewhere in the tail, is very similar to the situation for NGC 7252. It will be very interesting to see if the other two unreduced pointings on the NGC 4038/39 tails (see Figure 1) show a similar lack of bright clusters.

Clearly, the Western tail of NGC 3256 has the largest population of tail clusters observed in our sample. Both the colors and concentration of these objects are coincident with inner region clusters in the merger. The Eastern tail has a small excess ($\sim 2\sigma$) of clusters as well.

So why might the tails of NGC 3256 be a preferred environment for extensive cluster formation? The tails of NGC 3256 are very similar to other tails that do not show such large numbers of clusters; all show large numbers of inner region clusters; all are rich in atomic gas; all have dynamical ages from 400-800 Myr (with NGC 3256 and NGC 3921 at the lower range of that scale). However, NGC 3256 is extremely bright in the X-ray and far-IR, and also has the largest number of clusters in its inner regions.

From the far infrared luminosities of each pair, we calculated the global star formation rates using the relation of Kennicutt (1998b): $SFR = 4.5 \times 10^{-44} L_{FIR} M_{\odot} \text{ yr}^{-1}$. This conversion assumes that the dust re-emits all of the young starlight ($\tau \gg 1$), and that the dust heating is dominated by young stars, with ages of order 10^8 years or less. As shown in Table 4, NGC 3256 stands out clearly with a star formation rate several times that of the Antennae and NGC 7252, the next closest pairs. Though these rates are calculated from the integrated infrared luminosities rather than locally for the tidal tails, the overall enhancement of star formation in NGC 3256 may be a prerequisite for the efficient production of star clusters. Also, the star formation rate is related to the current burst of star formation and might not indicate the conditions in the merger when the star clusters in the tails formed, but perhaps the higher star formation rate of NGC 3256 indicates

a higher global molecular gas content that would aid in more efficient star cluster formation.

We should consider whether the specific frequency of young clusters is large for NGC 3256, or whether the number of young clusters is what would be expected based upon the luminosity of the tail region. From Whitmore & Schweizer (1995) and Goudfrooij et al. (2001), we can compare the specific frequency of young clusters forming in the central regions of mergers with S_{young} of our tidal tails. We calculated the M_V of the tidal tails by using the IRAF task IMSTAT at several typical locations within the tail, and subtracted the background, measured at several locations outside the tail. The Western tail of NGC 3256 has a very large specific frequency, $S_{young} = 2.5$, comparable to $S_{young}^6 \sim 2$ found in the central regions of NGC 4038/39 (Whitmore & Schweizer 1995) and $S_{young}^7 = 1.7$ found in NGC 1316 (Goudfrooij et al. 2001). Clearly, calculation of S_{young} is complicated by destruction of clusters, fading, etc. However, it is still quite interesting that one of these tails hosts clusters, that are as luminous, relative to stars as in central regions of merging galaxies.

Another difference between NGC 3256 and the other pairs, is that, unlike the other three systems, NGC 3256 does not have a prominent tidal dwarf galaxy associated with the tip of its tidal tail either in the optical image or in H I maps. A hypothesis, based on our admittedly small sample of six tidal tails, is that tails with prominent tidal dwarfs form fewer clusters than tails without such dwarfs. If we also consider the ACS early release observations of UGC 10214 and NGC 4676, they follow a similar trend. Although no correction was made for background contamination, UGC 10214 (which has a tidal dwarf candidate) has fewer star clusters in its tail than NGC 4676 (which does not host a tidal dwarf candidate) (de Grijs et al. 2003; Tran et al. 2003). However, UGC 10214 is thought to be a disturbed spiral with a single long tidal tail, a different environment from the merging pairs of spiral galaxies that comprise our sample and NGC 4676. UGC 10214 also hosts many young star clusters in the bright blue clump at the mid-point of

⁶This number corresponds to S in Whitmore & Schweizer (1995).

⁷This number corresponds to S_N in Goudfrooij et al. (2001).

its tail with ages from $\sim 3 - 10$ Myr (Tran et al. 2003).

Elmegreen & Efremov (1997) showed that large mass clumps and high specific kinetic energies lead to a higher efficiency for star formation because of an increased binding energy and resistance to disruption. Perhaps the details of the interaction (i.e. the mass of the perturber, the orbital properties of the two galaxies as they merge, the gas content of the parent galaxy, the dark matter distribution, and the velocity of the perturber) influence the process of star formation in the debris. We hypothesize that global characteristics of the encounters affect the local conditions, conspiring so that star clusters form along the tail or within a dwarf galaxy in the tail, but not both.

We thank the referee for a number of helpful comments and suggestions. Support for this work was provided by grant STSI NASA GO-07466.01-96A from the Space Telescope Science Institute, which is operated by AURA, Inc., under NASA contract NAS5-26555. Additional support was provided by the National Science Foundation under grant AST-0071223. KAK was also supported by an NSF REU Supplement.

REFERENCES

- Aalto, S., Black, J. H., Booth, R. S., & Johansson, L. E. B. 1991, *A&A*, 247, 291
- Ajhar, E. A., Blakeslee, J. P., & Tonry, J. L. 1994, *AJ*, 108, 2087
- Amram, P., Marcelin, M., Boulesteix, J., & le Coarer, E. 1992, *A&A*, 266, 106
- Arp, H. C. 1966, *Atlas of Peculiar Galaxies* (Pasadena: CalTech).
- Barnes, J. E. 1988, *ApJ*, 331, 699
- Barth, A. J., Ho, L. C., Filippenko, A. V., & Sargent, W. L. W. 1995, *AJ*, 110, 1009
- Bruzual, A. G., & Charlot, S. 1993, *ApJ*, 405, 538
- Casoli, F., Dupraz, C., Combes, F., & Kazes, I. 1991, *A&A*, 251, 1
- Charlot, S., Worthey, G., & Bressan, A. 1996, *ApJ*, 457, 625
- de Grijs, R., Lee, J. T., Mora Herrera, M. C., Fritze-v. Alvensleben, U., & Anders, P. 2003, *New Astronomy*, 8, 155
- Duc, P.-A., & Mirabel, I. F. 1994, *A&A*, 289, 83
- Duc, P.-A., & Mirabel, I. F. 1998, *A&A*, 333, 813
- Duc, P.-A., & Mirabel, I. F. 1999, in *Galaxy Interactions at Low and High Redshift*, IAU Symposium No. 186, eds. D. Sanders & J. Barnes, p. 61
- Elmegreen, B. G., & Efremov, Y. N. 1997, *ApJ*, 480, 235
- English, J., & Freeman, K. C. 2003, *AJ*, 125, 1124
- English, J., Norris, R. P., Freeman, K. C., & Booth, R. S. 2003, *AJ*, 125, 1134
- Fritze-v. Alvensleben, U. 1998, *A&A*, 336, 83
- Gallagher, S. C., Charlton, J. C., Hunsberger, S. D., Zaritsky, D. & Whitmore, B. C. 2001, *AJ*, 122, 163
- Goudfrooij, P., Alonso, M. V., Maraston, C., & Minniti, D. 2001, *MNRAS*, 328, 237
- Harris, W. E. 1991, *ARA&A*, 29, 543
- Harris, W. E., & Pudritz, R. E. 1994, *ApJ*, 429, 177
- Hibbard, J. E., Guhathakurta, P., van Gorkom, J. H., & Schweizer, F. 1994, *AJ*, 107, 67
- Hibbard, J. E., & Mihos, J. C. 1995, *AJ*, 110, 140
- Hibbard, J. E., & van Gorkom, J. H., 1996, *Astronomical Journal*, 111, 655
- Hibbard, J. E. 2000, private communication
- Hibbard, J. E., van der Hulst, T., Barnes, J. E., & Rich, R. M. 2001a, *AJ*, 122, 2969
- Hibbard, J. E., van Gorkom, J. H., Rupen, M. P., & Schiminovich, D. 2001b, in *ASP Conf. Ser. 240, Gas and Galaxy Evolution*, eds. J. E. Hibbard, M. P. Rupen and J.H. van Gorkom (ASP, San Francisco), 659
- Holtzman et al. 1992, *AJ*, 102, 691
- Holtzman et al. 1995, *PASP*, 107, 1065

- Hunsberger, S. D., Charlton, J. C., & Zaritsky, D. 1996, *ApJ*, 462, 50
- Iglesias-Páramo, J., & Vílchez, J. M. 2001, *ApJ*, 550, 204
- Jog, C. J., & Solomon, P. M. 1992, *ApJ*, 387, 152
- Kennicutt, R. C. 1992, *ApJ*, 388, 310
- Kennicutt, R. C. 1998, in *Induced Star Formation, Galaxies: Interactions and Induced Star Formation* (Berlin: Springer)
- Kennicutt, R.C. 1998, *ARA&A*, 36, 189
- Kennicutt, R. C., Roettiger, K. A., Keel, W. C., van der Hulst, J. M., & Hummel, E. 1987, *AJ*, 93, 1011
- Knapp, G. R., Guhathakurta, P., Kim, D., & Jura, M. A. 1989, *ApJS*, 70, 329
- Kundu, A. 1999, Ph.D. Thesis, University of Maryland
- Kundu, A., Whitmore, B. C., Sparks, W. B., Macchetto, F. D., Zepf, S. E., & Ashman, K. M. 1999, *ApJ*, 513, 733
- Kundu, A., & Whitmore, B. C. 2001, *AJ*, 121, 2950
- Kundu, A., & Whitmore, B. C. 2001, *AJ*, 122, 1251
- Larsen, S. S., & Richtler, T. 1999, *A&A*, 345, 59
- Lee, H., Lee, Y. & Gibson, B. K. 2002, *AJ*, 124, 2664
- Mathis, J. S. 1990, *ARA&A*, 28, 37
- Meurer, G. R., Heckman, T. M., Lietherer, C., Kinney, A., Robert, C., & Garnett, D. R. 1995, *AJ*, 110, 2665
- Miller, B., Whitmore, B., Schweizer, F., & Fall, S.M. 1997, *AJ*, 114, 2381
- Mirabel, I. F., Booth, R. S., Johansson, L. E. B., Garay, G., & Sanders, D. B. 1990, *A&A*, 236, 327
- Mirabel, I. F., Dottori, H., & Lutz, D. 1992, *A&A*, 256, L19
- Moran, E. C., Lehnert, M. D., & Helfand, D. J., 1999, *ApJ*, 526, 649
- Moshir, M. & et al. 1990, *IRAS Faint Source Catalogue*, version 2.0 (1990)
- Norris, R. P., & Forbes, D. A. 1995, *ApJ*, 446, 594
- Peterson, C. J. 1993, in *Structure and Dynamics of Globular Clusters*, edited by S. G. Djorgovsky and G. Meylan (PASP, San Francisco), p. 337
- Press, W. H., Flannery, B. P., Teukolsky, S. A., & Vetterling, W. T. 1986, *Numerical Recipes: The Art of Scientific Computing* (Cambridge University Press)
- Ranalli, P., Comastri, A., & Setti, G. 2003, *A&A*, 399, 39
- Reed, B. C., Hesser, J. E., & Shawl, S. J. 1988, *PASP*, 100, 545
- Sargent, A. I., Sanders, D. B., & Phillips, T. G. 1989, *ApJ*, 346, L9
- Saviane, I., Hibbard, J. E. & Rich, R. M. 2003, *AJ*, submitted
- Schlegel, D. J., Finkbeiner, D. P., & Davis, M. 1998, *ApJ*, 500, 525
- Schombert, J. M., Wallin, J. F., & Struck–Marcell, C. 1990, *AJ*, 99, 497
- Schweizer, F. 1978, in *Structure and Properties of Nearby Galaxies*, ed. E. M. Berkhuysen & R. Wielebinski (Reidel, Dordrecht), 279
- Schweizer, F. 1982, *ApJ*, 252, 455
- Schweizer, F. 1996, *AJ*, 111, 109
- Schweizer, F., Miller, B., Whitmore, B., & Fall, S. M. 1996, *AJ*, 112, 1839 (S96)
- Schweizer, F. 1998, in *Observational Evidence for Interactions and Mergers, Galaxies: Interactions and Induced Star Formation* (Berlin: Springer)
- Schweizer, F., & Seitzer, P. 1998, *AJ*, 116, 2206
- Tran, H. D., et al. 2003, *ApJ*, 585, 750

- Toomre, A. 1977, in *The Evolution of Galaxies and Stellar Populations*, edited by B. M. Tinsley and R. B. Larson (New Haven: Yale Univ.), p. 401
- Toomre, A., & Toomre, J. 1972, *ApJ*, 178, 623
- van den Bergh, S. 1996, *AJ*, 112, 2634
- van den Bergh, S. 1995, *Nature*, 374, 215
- van der Hulst, J. M. 1979, *A&A*, 155, 151
- Voit, M. 1997, *HST Data Handbook* (Space Telescope Science Institute, Baltimore)
- Wang, Z., Schweizer, F., & Scoville, N. Z. 1992, *ApJ*, 396, 510
- Weilbacher, P. M., Duc, P.-A., Fritze-v.Alvensleben, U., Martin, P., & Fricke, K. J. 2000, *A&A*, 358, 819
- Weilbacher, P. M., Duc, P.-A., & Fritze-v.Alvensleben, U. 2003, *A&A*, 397, 545
- Whitmore, B. C., Miller, B. W., Schweizer, F., & Fall, S. M. 1997, *AJ*, 114, 1802
- Whitmore, B. C., Schweizer, F., Leitherer, C., Borne, K., & Robert, C. 1993, *AJ*, 106, 1354
- Whitmore, B. C., & Schweizer, F. 1995, *AJ*, 109, 960
- Whitmore, B. C., Sparks, W. B., Lucas, R. A., Macchetto, F. D., & Biretta, J. A. 1995, *ApJ*, 454, L73
- Whitmore, B. C., Heyer, I., & Casertano, S. 1999, *PASP*, 111, 1559
- Whitmore, B. C., Zhang, Q., Leitherer, C., Fall, S. M., Schweizer, F., & Miller, B. 1999, *AJ*, 118, 1551
- Yun, M. S., Ho, P. T. P., & Lo, K. Y. 1994, *Nature*, 372, 530
- Zepf, S., Ashman, K., English, J., Freeman, K., & Sharples, R. 1999, *AJ*, 118, 752
- Zhang, Q., & Fall, S. M. 1999, *ApJ*, 527, L81

Figures

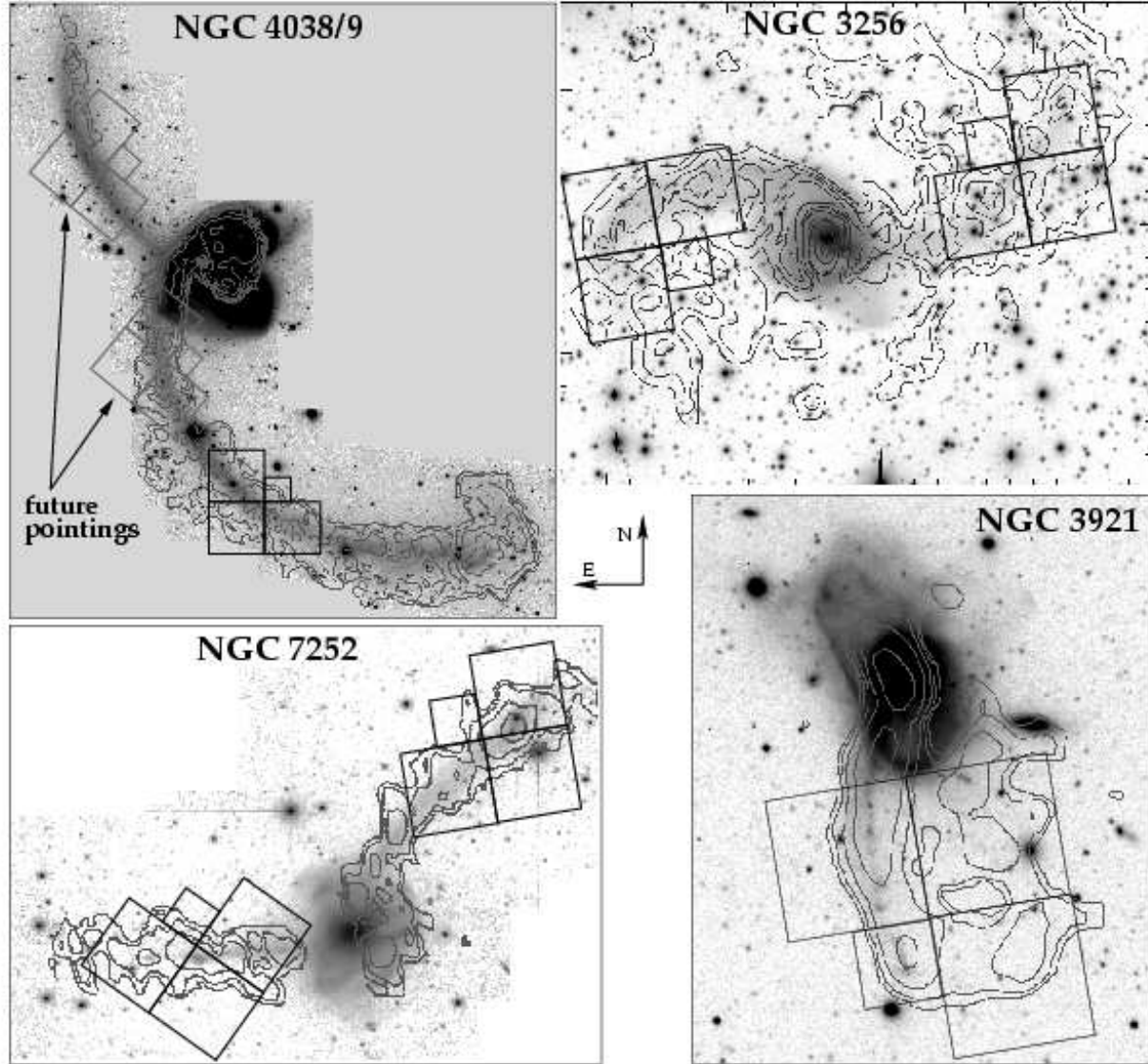


Fig. 1.— Upper left — Optical image in BVR of early stage remnant NGC 4038/39 (“Antennae”) from the CTIO 0.9m with integrated H I line emission, shown as overlaid contours taken with the VLA C+D arrays (Hibbard et al. 2001a). The HST WFPC2 field of view of our 1999 Feb 22 observations is indicated by black boxes, and our two later observations (not analyzed here) are indicated by gray boxes; Upper right — Optical image of NGC 3256, from UH88” R -band. The HST WFPC2 fields of view of our observations are indicated by the black boxes. H I data have been obtained at ATCA (English et al. 2003).; Lower left — Optical image of NGC 7252, from CTIO 4m R_j -band, with H I contours overlaid (Hibbard & van Gorkom 1996). Lower right — Optical image of NGC 3921, KPNO 0.9m R -band image, with integrated H I line emission, shown in overlaid contours taken with the VLA C+D arrays (Hibbard & van Gorkom 1996).

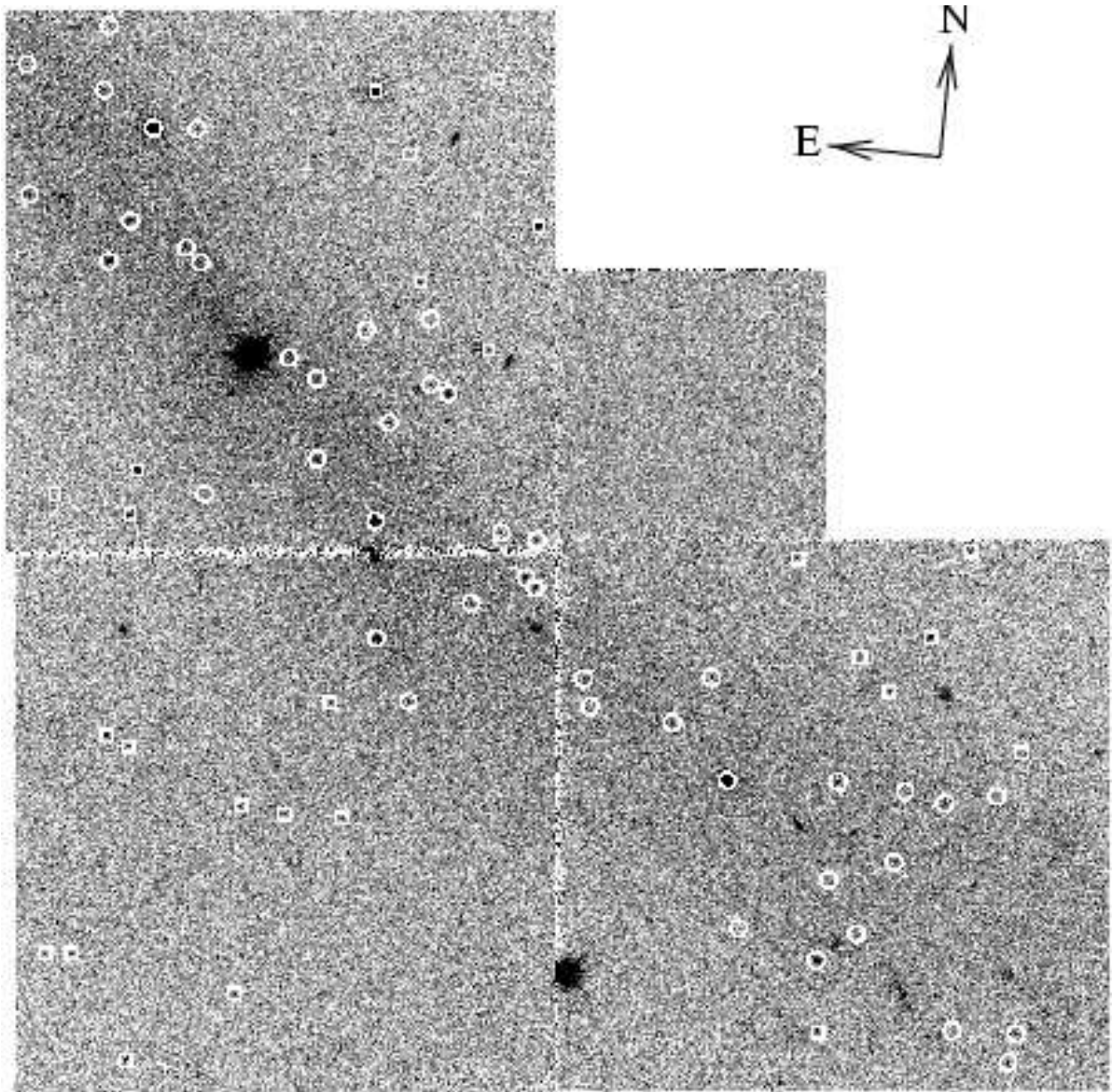


Fig. 2.— HST WFPC2 image of NGC 4038/39 (“Antennae”) Southern tail taken with F555W (V) filter. Circles indicate sources in the tail and squares indicate those outside of the tail. Sources within the tail are likely to be individual stars and not clusters.

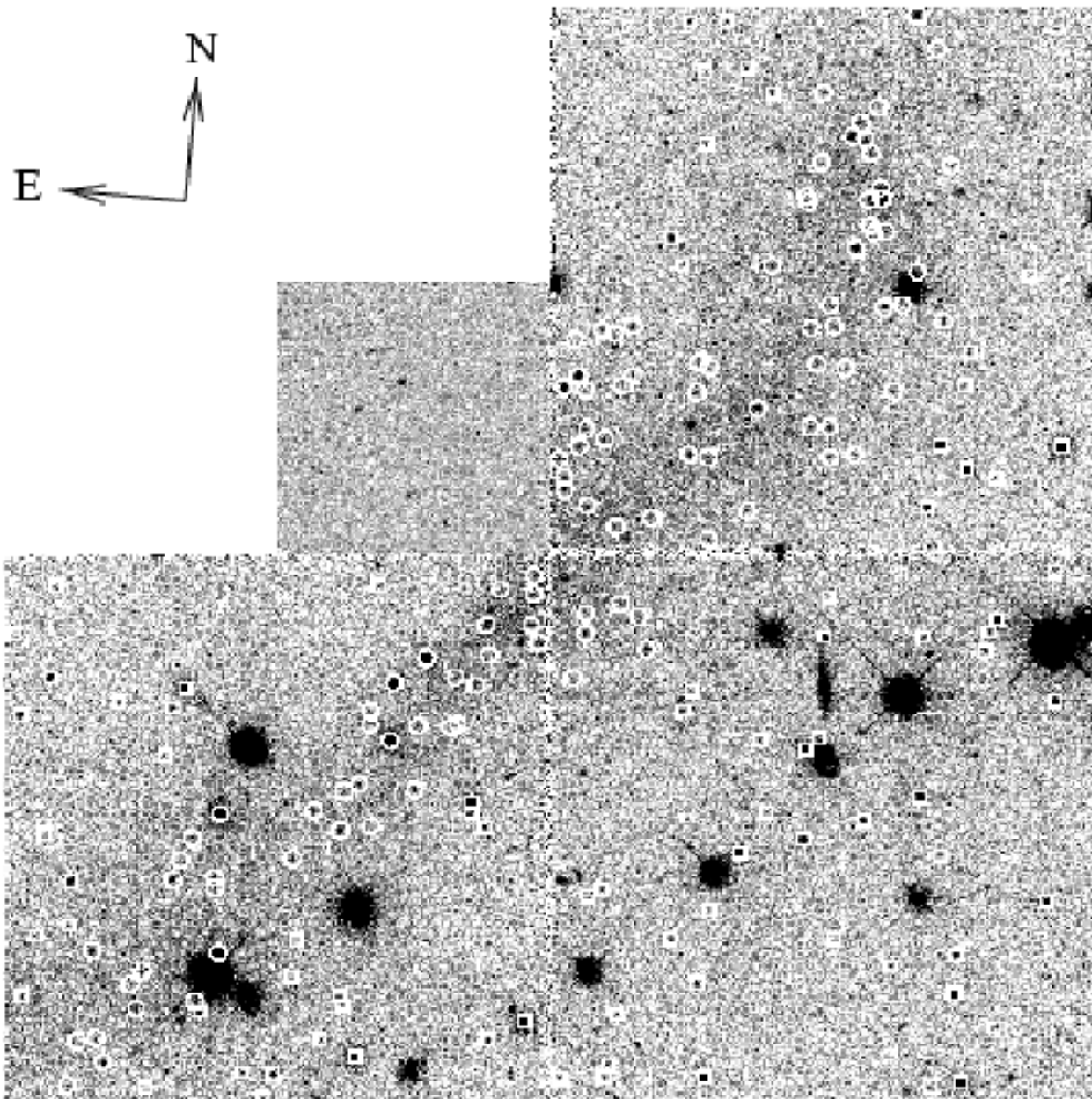


Fig. 3.— HST WFPC2 image of NGC 3256 Western Tail taken with the F555W (V) filter. Circles indicate sources within the tail and squares indicate those outside the tail. The majority of sources within the tail are likely to be clusters; note the large number.

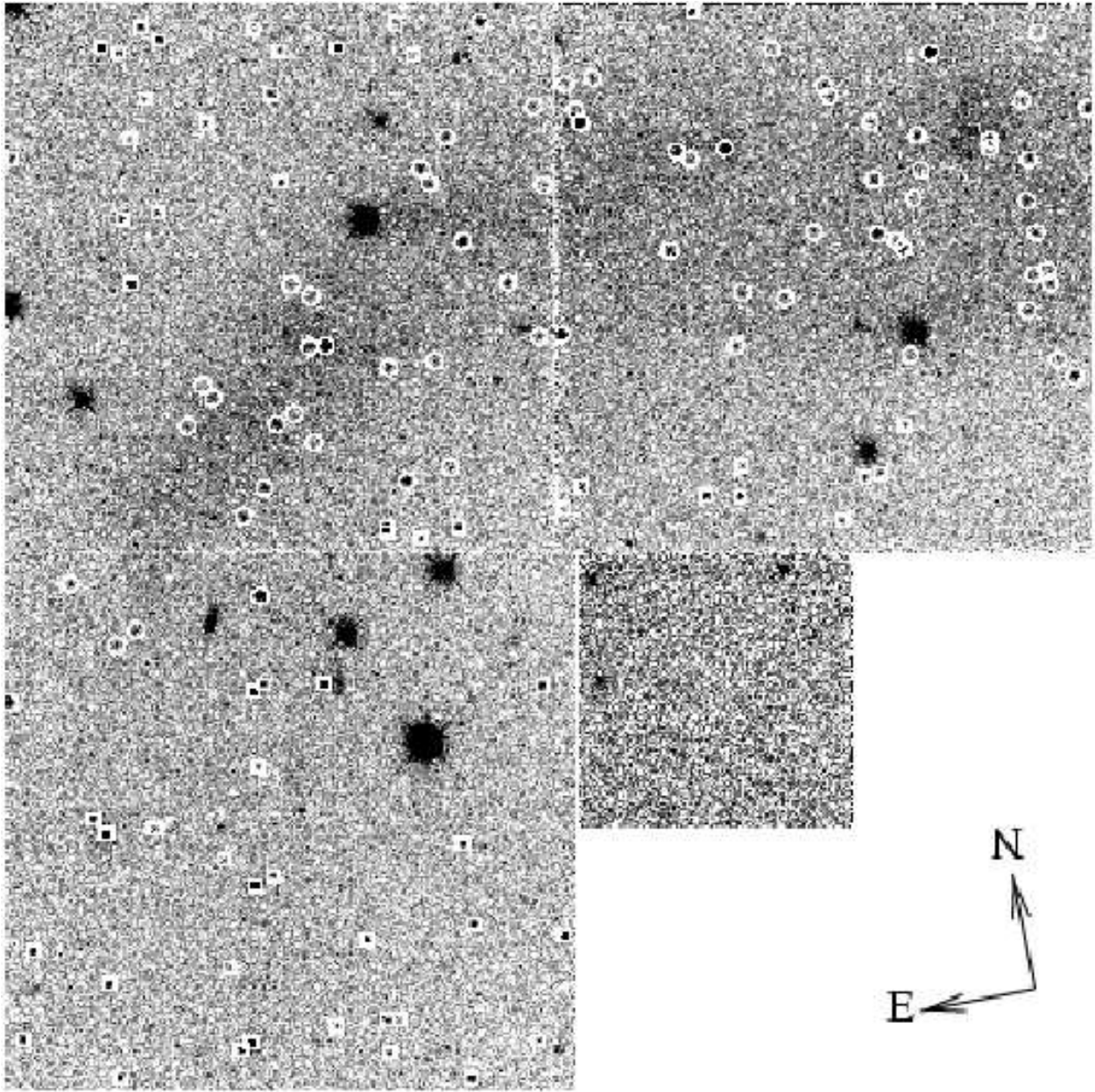


Fig. 4.— HST WFPC2 image, as in Figure 3, for NGC 3256 Eastern Tail, taken with F555W (*V*) filter.

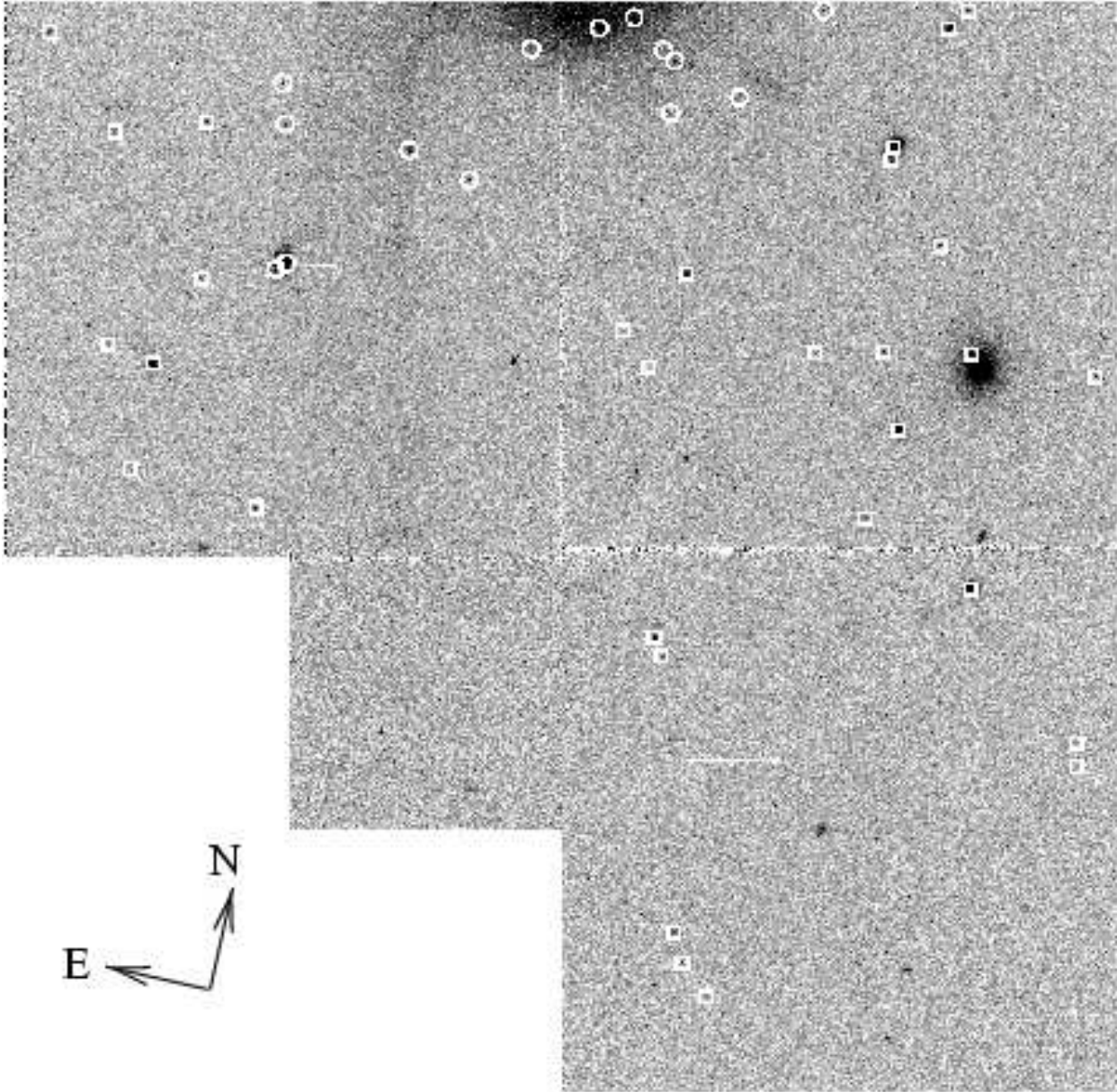


Fig. 5.— HST WFPC2 image of NGC 3921 Southern Tail, taken with F555W (V) filter. Circles indicate sources within the tail and squares indicate those outside the tail.

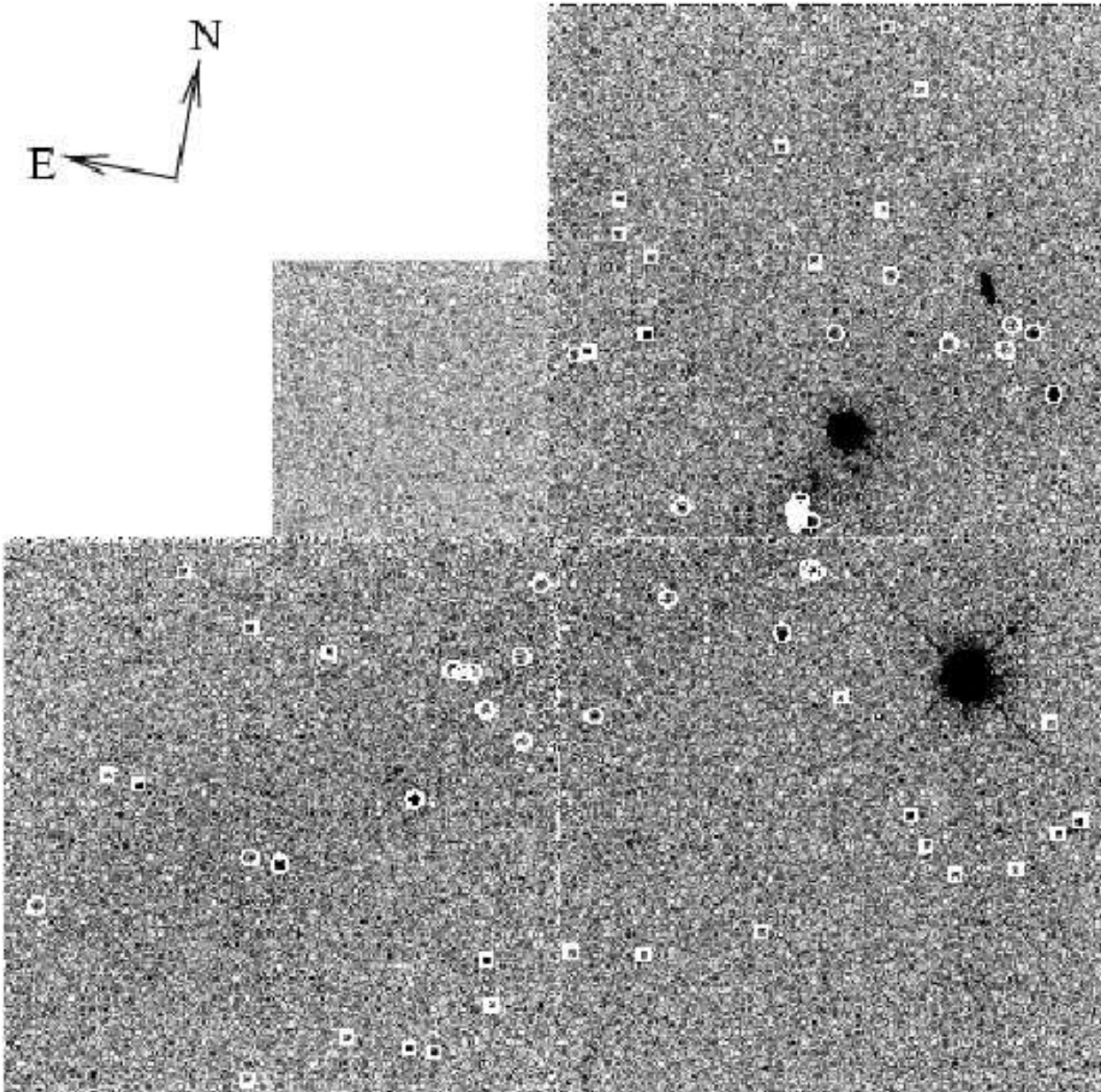


Fig. 6.— HST WFPC2 image of NGC 7252 Western Tail, taken with F555W (V) filter. Circles indicate sources within the tail and squares indicate those outside the tail.

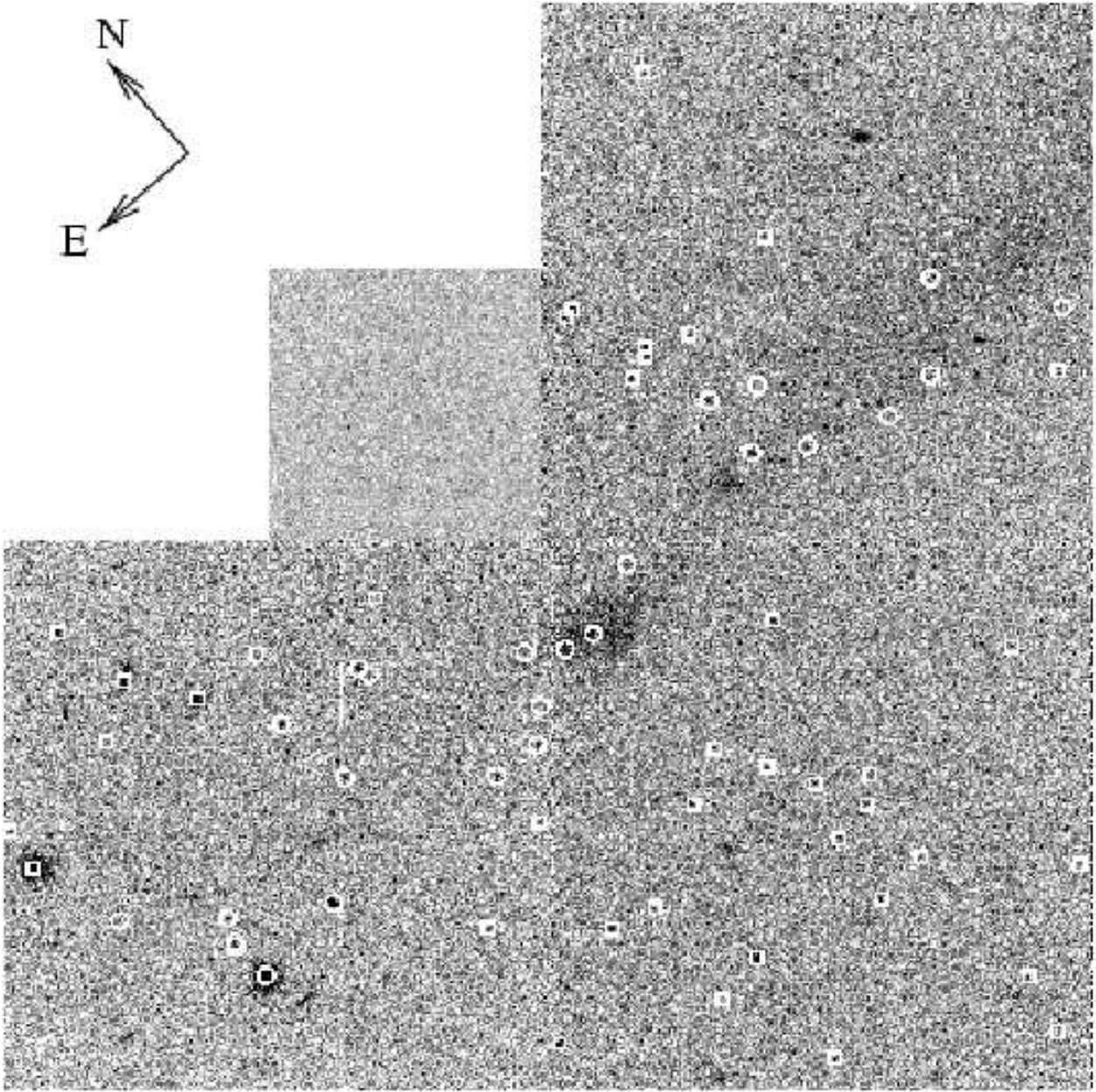


Fig. 7.— HST WFPC2 image, as in Figure 6, for NGC 7252 Eastern Tail, taken with F555W (*V*) filter.

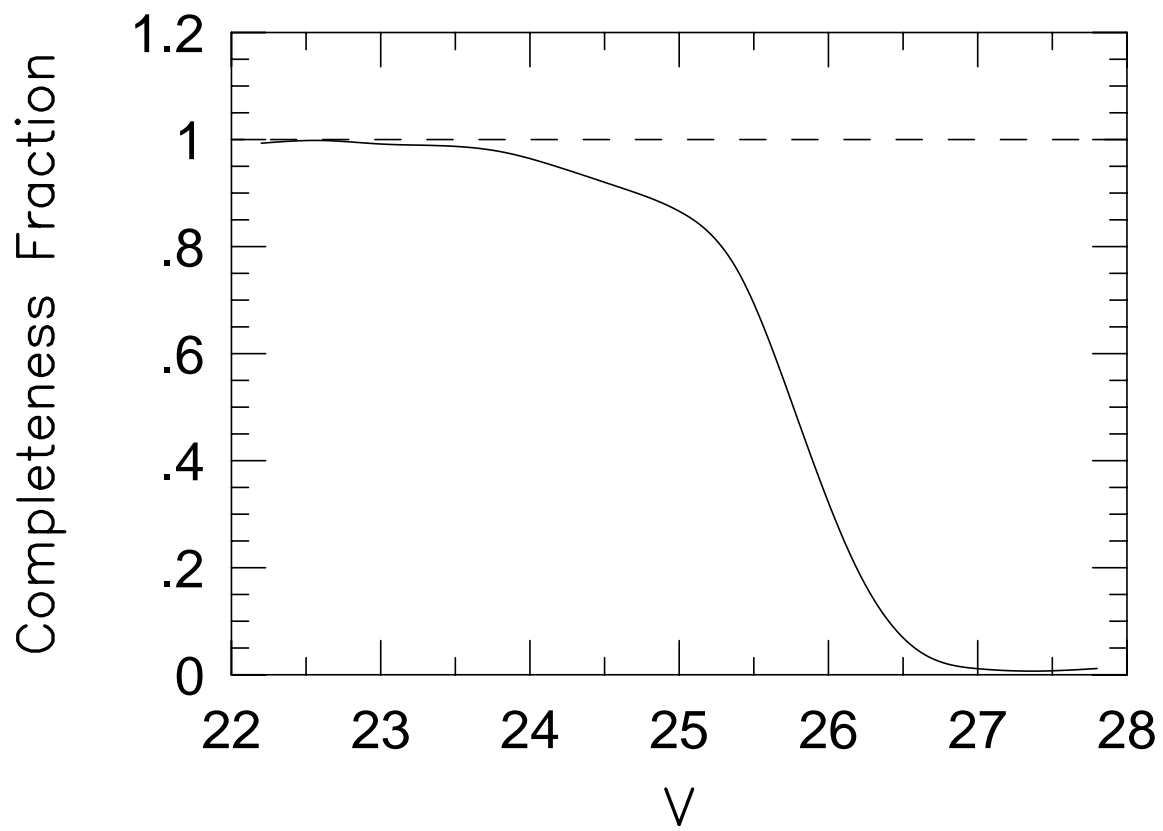


Fig. 8.— The completeness fraction for point sources as a function of the V magnitude, determined by adding artificial sources to the WF images of the NGC 3256 Western tail.

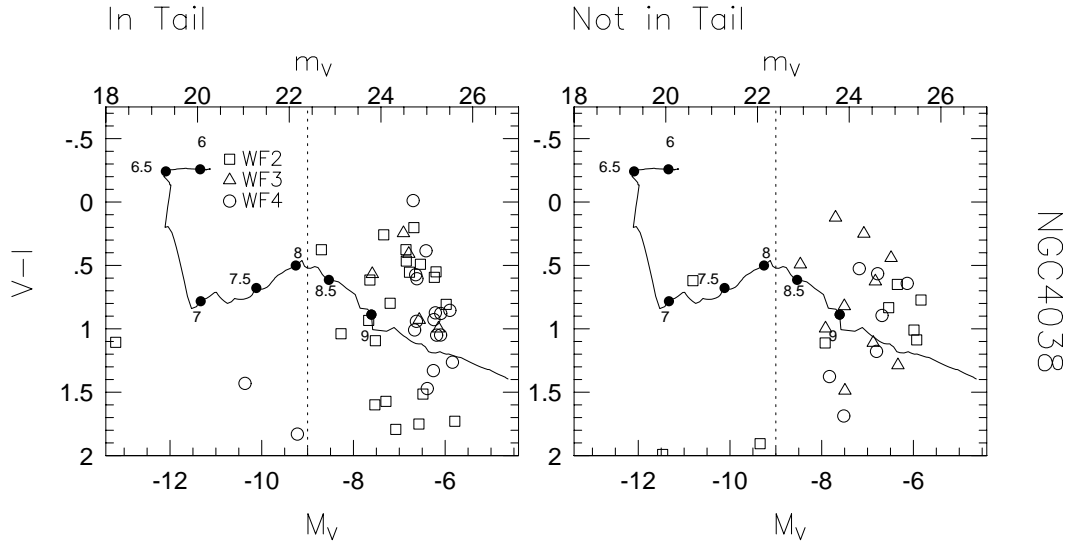


Fig. 9.— Color magnitude diagram for sources in and out of the tail region of NGC 4038. Color $V - I$ is plotted versus absolute magnitude M_V , on the lower horizontal scale, and apparent magnitude V , on the upper horizontal scale. The absolute magnitude scale enables comparison between different tails. All sources, both in and outside of the tail, with errors in V less than 0.25 magnitudes and with $-0.75 < V - I < 2.0$, are included. Sources coming from the different WF chips are identified by special symbols as indicated in the legend. No corrections have been made for incompleteness. The vertical dashed line indicates a rough boundary such that brighter sources are more likely to be clusters, rather than individual stars. The curve represents the evolutionary track for an instantaneous burst model for a $10^5 M_\odot$ cluster with solar metallicity and a Salpeter IMF with a $125 M_\odot$ cutoff, marked with $\log(\text{age})$ in years (Bruzual & Charlot 1993; Charlot, Worthey, & Bressan 1996). This model would shift by a magnitude horizontally for every factor of 2.5 in mass.

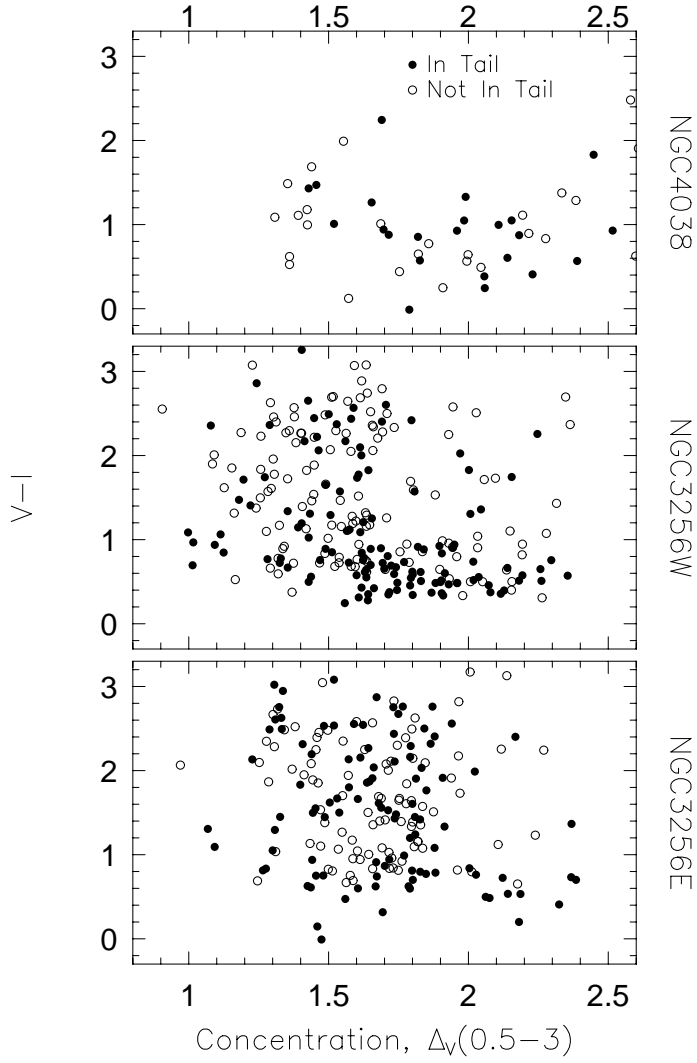


Fig. 10.— Concentration index plots for the two nearest mergers, NGC 4038 and NGC 3256 (Western and Eastern tails). Color $V - I$ is plotted versus concentration index $\Delta_V(0.5 - 3)$. The concentration index (a rough measure of cluster size) was calculated from the difference in V magnitude between an aperture of 0.5 and 3.0 pixel radii. Sources within the tail are indicated by solid circles, while those outside the tail are indicated by open circles.

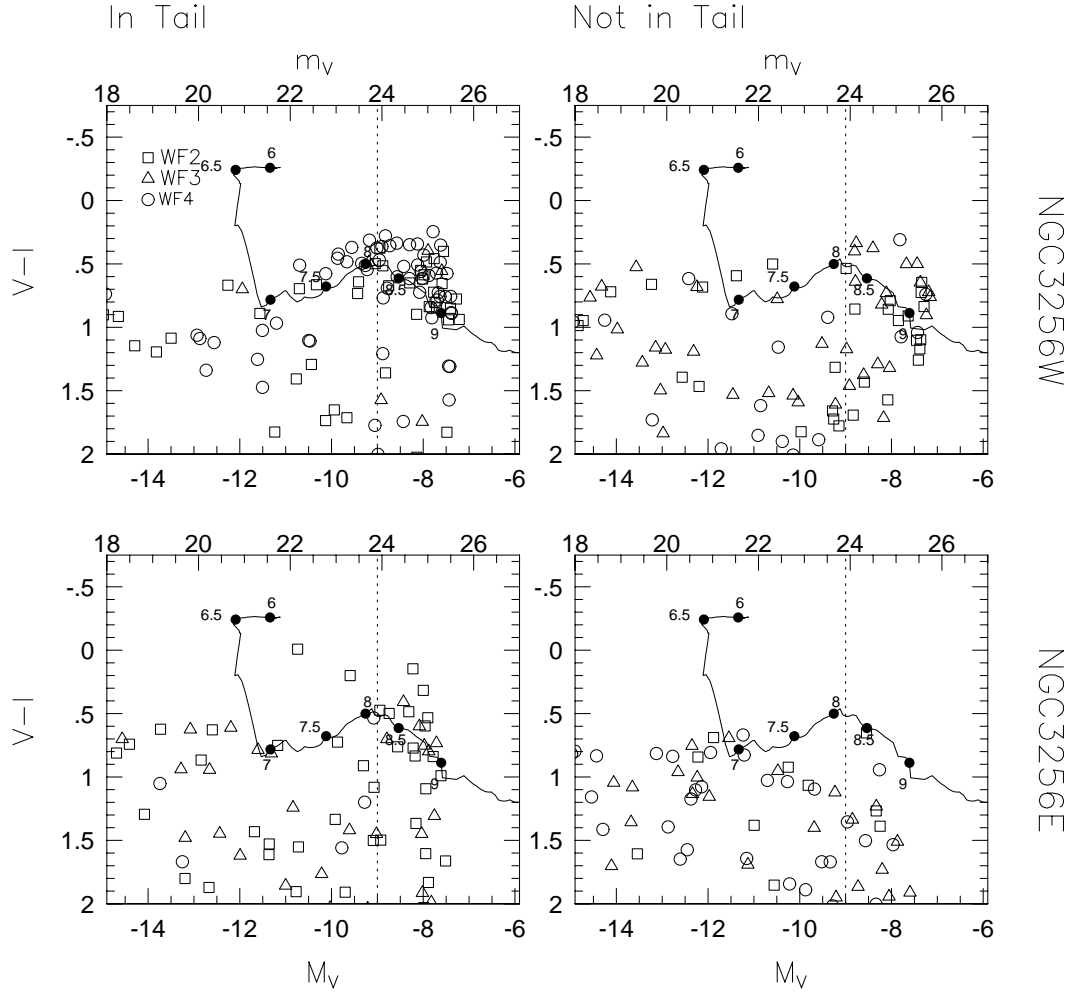


Fig. 11.— Color magnitude diagrams, same as Figure 9, but for NGC 3256. The Western and Eastern sources, in and out of the tails, are given in the top and bottom rows, respectively.

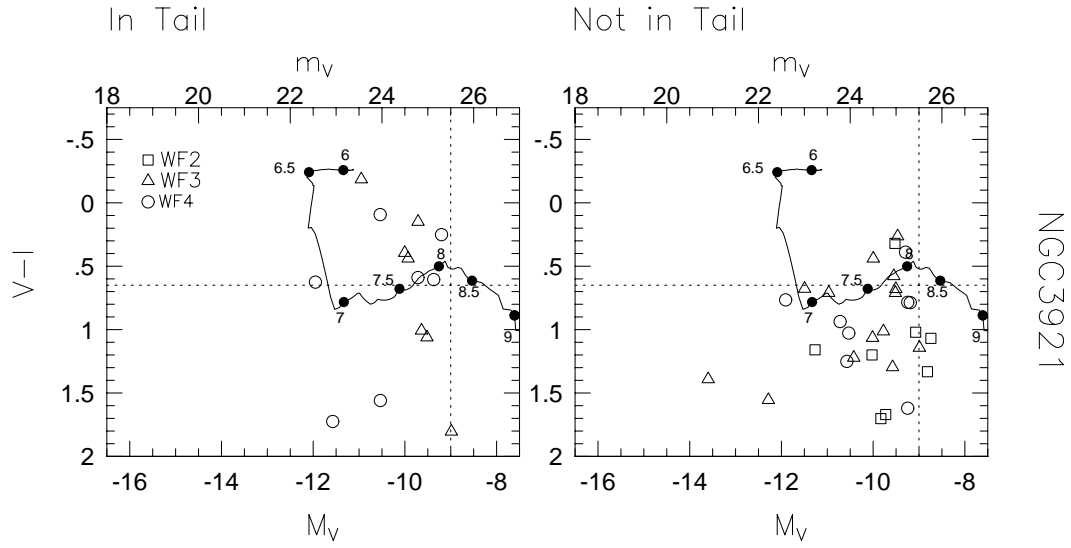


Fig. 12.— Same as Figure 9, but for NGC 3921. The horizontal line represents the median $V - I$ for the clusters in the inner region of the merger.

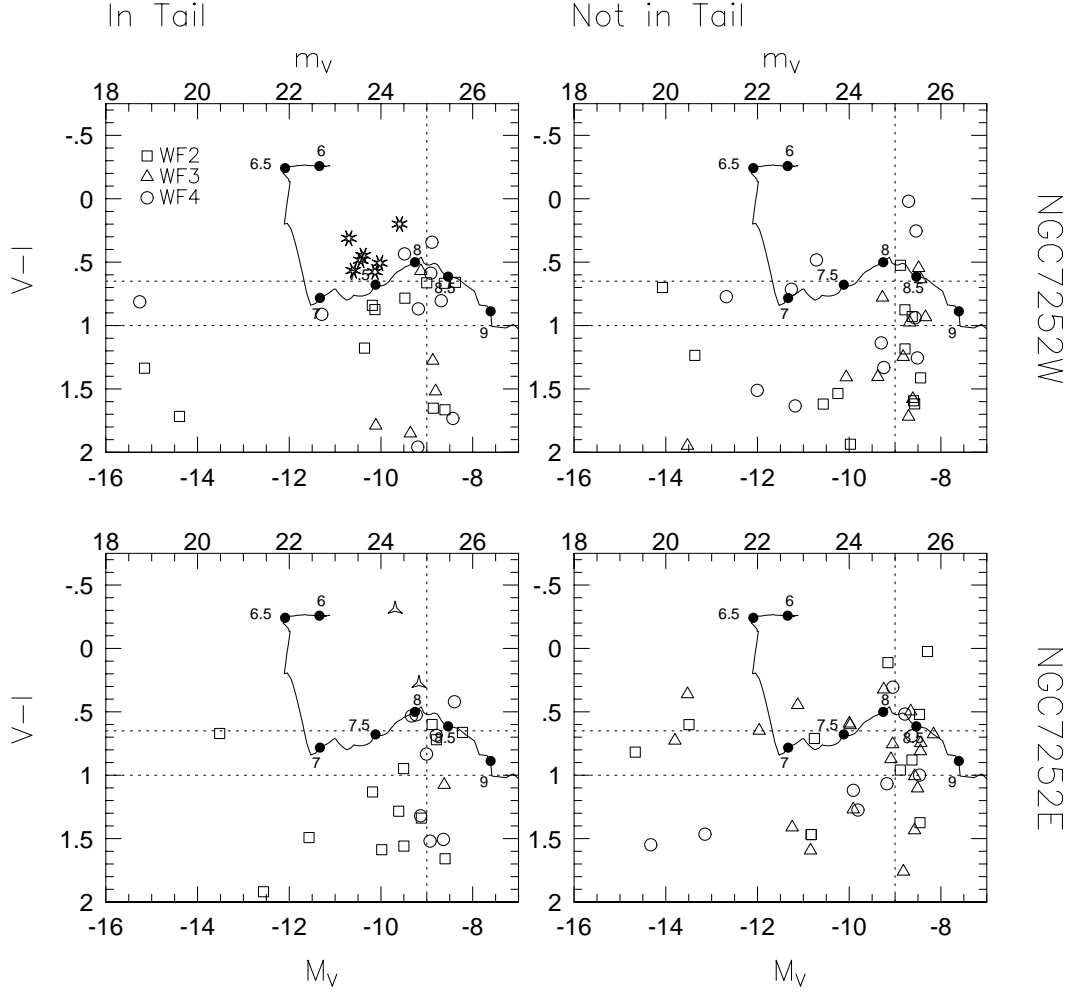


Fig. 13.— Same as Figure 9, but for NGC 7252. The Western and Eastern sources, in and out of the tails, are given in the top and bottom rows, respectively. The sources in the tidal dwarfs at the end of the Western and Eastern tails (see Figure 14) are indicated as “star symbols” of the shape corresponding to the appropriate WF chip. For comparison, the horizontal dotted lines represent the colors of the two main populations of clusters in the inner region of this merger. The evolutionary track for a single burst Bruzual and Charlot model (Bruzual & Charlot 1993) is given as in previous CMDs.

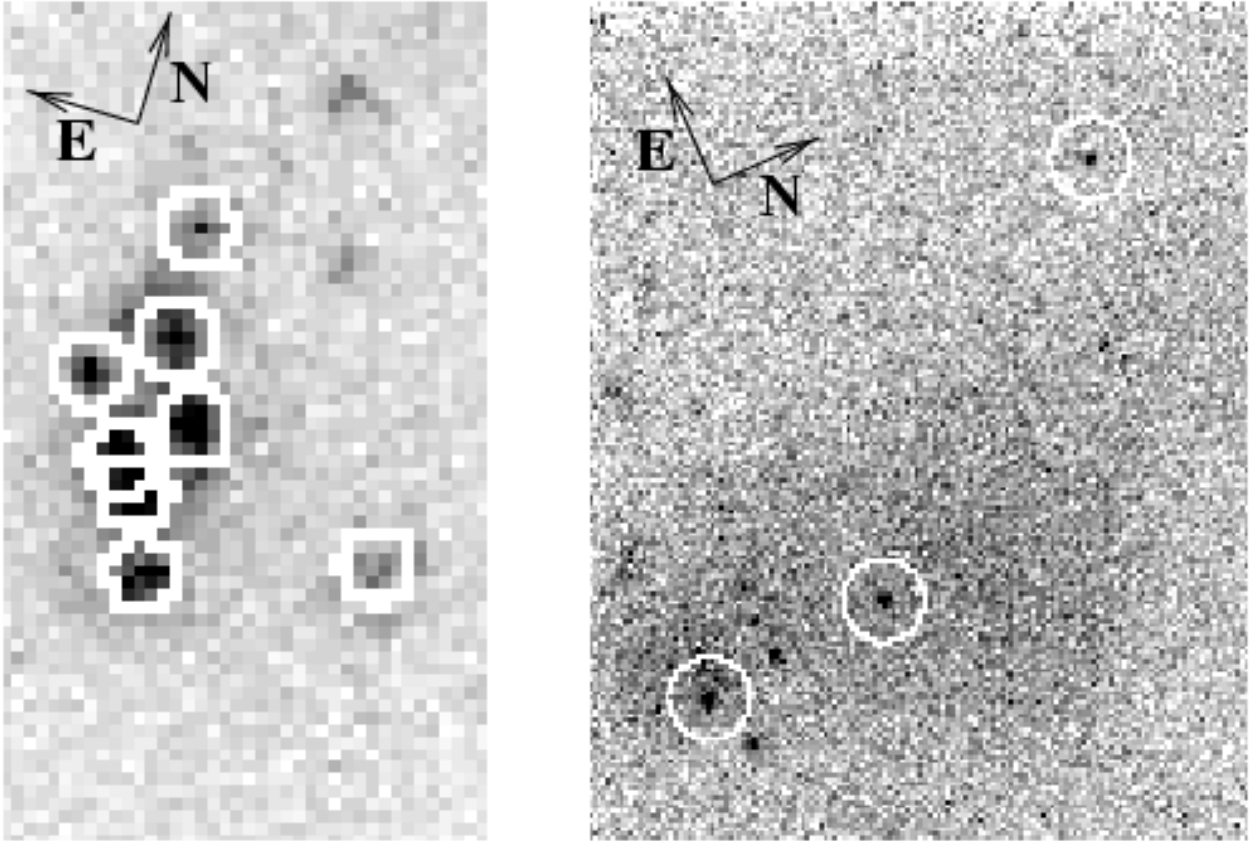


Fig. 14.— The dwarf galaxies at the ends of the Western (left) and Eastern (right) tails of NGC 7252, taken in the F555W (V) filter. The colors and magnitudes of several clusters within these dwarfs are shown as “star symbols” in the CMDs of Figure 13. The clusters in the Western dwarf are found to be relatively blue ($V - I \sim 0.4$), somewhat younger than the dominant population in the inner region which has an age of $\sim 650\text{--}750$ Myr. Those in the Eastern tail are extremely blue ($V - I < 0.3$), consistent with the youngest population in the inner regions, having an age of ~ 10 Myr.

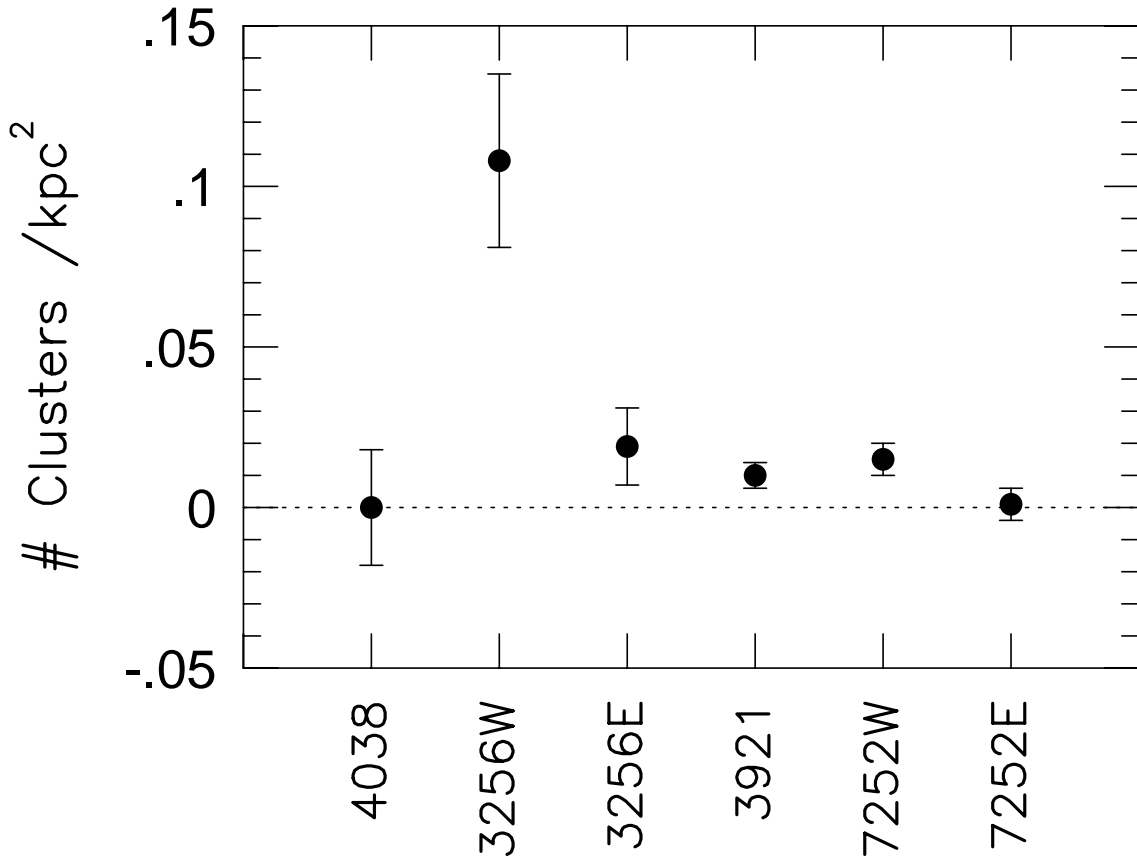


Fig. 15.— The number of candidate clusters per square kpc is compared for the six different areas of debris. Background sources were subtracted, statistically, using the source densities in areas “out-of-tail”. The excesses “in-tail” are plotted. Details of the calculation are given in Table 3.

TABLE 1
JOURNAL OF OBSERVATIONS

Tidal Tail	Filter	Time s	Date
NGC4038	F555W	2000	22 Feb 99
NGC4038	F814W	1800	22 Feb 99
NGC3256W	F555W	1000	24 Mar 99
NGC3256W	F814W	1000	24 Mar 99
NGC3256E	F555W	1000	11 Oct 99
NGC3256E	F814W	1000	11 Oct 99
NGC3921S	F555W	1800	30 Apr 99
NGC3921S	F814W	1600	30 Apr 99
NGC7252W	F555W	2000	18 Nov 98
NGC7252W	F814W	1800	18 Nov 98
NGC7252E	F555W	2000	29 Aug 99
NGC7252E	F814W	1800	29 Aug 99

TABLE 2
SUMMARY OF TIDAL TAIL PROPERTIES

Tidal Tail	Vel km s ⁻¹	Dist. Mod. mag	A_B^a mag	l kpc	Δl kpc	$M_{V,50\%}^b$ mag	$M_{HI,tail}$ M _⊙	Tail Age Myrs
NGC4038	1439	31.4	0.200	30	20	-5.8	2.0×10^8	420
NGC3256W	2820	32.9	0.524	15	40	-7.5	2.2×10^9	400
NGC3256E	2820	32.9	0.524	15	30	-7.5	1.4×10^9	400
NGC3921S	6021	34.5	0.062	0	45	-8.7	4.3×10^9	460
NGC7252W	4828	34.0	0.130	20	50	-8.1	2.2×10^9	730
NGC7252E	4828	34.0	0.130	0	60	-8.1	1.5×10^9	730

^aFrom Schlegel et al. (1998).

^bLimiting magnitude for $\sim 50\%$ completeness.

TABLE 3
SOURCE DENSITIES IN AND OUT OF DEBRIS

Tidal Tail	Pixel Size pc	N_{out}	f_{out}	N_{out}/Area kpc^{-2}	N_{in}	f_{in}	N_{in}/Area kpc^{-2}	Surplus	Spec. Freq.
NGC4038	8.92	1	0.501	0.013 ± 0.013	1	0.499	0.013 ± 0.013	0.000 ± 0.018	0.0
NGC3256W	18.2	12	0.677	0.028 ± 0.008	28	0.323	0.136 ± 0.026	0.108 ± 0.027	2.5
NGC3256E	18.2	4	0.538	0.012 ± 0.006	9	0.462	0.031 ± 0.010	0.019 ± 0.012	0.4
NGC3921S	38.8	7	0.751	0.003 ± 0.001	9	0.249	0.013 ± 0.004	0.010 ± 0.004	0.2
NGC7252W	31.1	5	0.623	0.004 ± 0.002	13	0.377	0.019 ± 0.005	0.015 ± 0.005	1.1
NGC7252E	31.1	13	0.618	0.011 ± 0.003	7	0.382	0.010 ± 0.004	-0.001 ± 0.005	-0.2

TABLE 4
STAR FORMATION RATES OF MERGING PAIRS

Pair	F_{FIR} $\text{erg cm}^{-2} \text{ s}^{-1}$	SFR $\text{M}_{\odot} \text{ yr}^{-1}$
NGC4038/9 ^a	2.6×10^{-9}	5.2
NGC3256 ^b	4.32×10^{-9}	33.4
NGC3921 ^b	$(2.69 - 5.25) \times 10^{-11}$	1.9
NGC7252 ^c	2.37×10^{-10}	5.4

^aFrom Ranalli, Comastri, & Setti (2003).

^bFrom Moshir et al. (1990).

^cFrom Knapp et al. (1989).